6. Introduction

Damage to the peripheral nervous system (PNS) can result in the development of atypical painful conditions collectively known as neuropathic pain (NP) (Colloca, Ludman et al. 2017). It involves an overlay of multiple pathophysiological alterations in the PNS and CNS, resulting in peripheral and central sensitization (Meacham, Shepherd et al. 2017). NP is a multifaceted and complicated phenomenon that encompasses numerous pain syndromes with different etiology, but they often have common symptoms such as heightened sensitivity to pain triggered by non-painful stimuli, with sudden and unpredictable pain episodes and abnormal sensations (Colloca, Ludman et al. 2017, Bannister, Sachau et al. 2020). Further, studies have demonstrated that neuropathy causes alterations in the expression of ion channels in the affected nerves, resulting in neuroplastic changes in the spinal and supraspinal tracts (Baron 2006). These changes play a significant role in the development and persistence of NP. It entails an aberrant increase in the intracellular calcium level [$(Ca^{2+})_i$], which further contributes to the pathogenesis of the disease (Siau and Bennett 2006, Cui, Wu et al. 2021). Currently, the primary pharmacological approaches for clinically managing chronic NP involve the use of calcium channel blockers (CCBs) such as pregabalin and gabapentin (Tong, Zhengyao et al. 2021). The efficacy of gabapentinoids (GBP) has been demonstrated clinically and in several preclinical NP models (Verma, Singh et al. 2014, Derry, Bell et al. 2019, Forouzanfar, Tanha et al. 2023). Previous studies have shown that GBP binds to the auxiliary unit of calcium channels and effectively reduces the central release of excitatory neurotransmitters, causing hyperexcitability of the nociceptors leading to hyperalgesia and allodynia (Patel and Dickenson 2016). All the CCBs that are currently used are organic compounds and the primary and common

adverse effects identified in GBP that result in its discontinuation in clinical usage are associated with the increased likelihood of atrial fibrillation along with somnolence and dizziness (Park, Hunter et al. 2023). Therefore, it is imperative to develop novel therapeutic approaches targeting calcium channels to effectively treat NP.

Barium is a rare trace element present in the human body (22 mg in a 70 kg adult) (Schroeder, Tipton et al. 1972), mainly in the bones and also in muscle, skin, connective tissue, and the lungs and elicits various physiological functions (Satoh, Kubota et al. 1987, Majumdar, Gupta et al. 2021, Majumdar, Hira et al. 2021). According to reports, barium is found in exoplanets, indicating that all living organisms have developed with barium in their bodies (Silva, Demangeon et al. 2022). In addition, barium is found in rocks, soil, and water (Myrvang, Gjengedal et al. 2016), meaning that every living organism is inevitably exposed to barium. Thus, our body has mechanisms to utilize as well as eliminate it, unlike the organic compounds that are foreign to the body. Previously, fewer reports indicated that the presence of Ba^{2+} in the extracellular fluid resulted in prolonged action potential plateaus observed in the growth cone of regenerating axon of lamprey (Macvicar's and Llinas 1985). Barium is also reported to generate a barium spike in the growth cone of the regenerating axon (Macvicar's and Llinas 1985). Besides, the calcium channels exhibit greater selectivity for Ba^{2+} ions compared to Ca^{2+} ions (Hagiwara and Byerly 1981). In light of the aforementioned facts, we have selected inorganic barium-doped bioactive glass (BaBG) in our current investigation. BaBG is safe and devoid of organ toxicity (Majumdar and Krishnamurthy 2022) as mentioned in **Chapter 4**. BaBG also possesses regenerative potential, as observed in the scratch assay which is an *in-vitro* transection model of neurotrauma (Majumdar, Hira et al. 2021). Additionally, our previous studies have established the

anti-inflammatory properties of BaBG, which have been extensively discussed in detail in **Chapter 2** and NP development is closely linked with neuroinflammation (Ellis and Bennett 2013, Teixeira-Santos, Albino-Teixeira et al. 2020). Further, in our previous preliminary work, the BaBG scaffold (Indian patent No.: 484408) has exhibited the ability to regenerate the deafferented nerve in the complete transection model of NP. Therefore, BaBG has the potential to be used for the treatment of NP which would probably act on the calcium channels and CCBs are widely used for the management of NP.

Further, in **Chapter 5**, we have observed that there was a time-dependent increase in the intracellular calcium and S100b levels in the CCI-induced NP model. Besides, S100b induces the aberrant release of pro-inflammatory cytokines that are involved in the development and progression of NP phenotypes (Tanga, Raghavendra et al. 2006, Stefani, Leite et al. 2019). In addition, prior research has shown that the presence of Ba^{2+} inhibits the release of S100b from primary astrocyte cultures (Vizuete, Hansen et al. 2019). Consequently, we believe that barium leached from the BaBG has the potential to mitigate the S100-induced neuroinflammation, a crucial factor involved in the persistence of NP.

To validate our hypothesis, in the present study, NP was induced by chronic constriction injury (CCI) of sciatic nerve (SN) in rats and the effect of BaBG on the development of the sensory hypersensitivity and characteristic motor impairment observed in NP were evaluated for the first time by various behavioral tests. Then the calcium-regulating mechanism of BaBG was elucidated in the *ex vivo* electrophysiology set-up. Additionally, the effects of BaBG on the $(Ca^{2+})_i$ and S100b level were evaluated post-CCI injury. Following this, we measured the severity of neuroinflammation developed

in this model and assessed the impact of BaBG on the level of pro-inflammatory cytokines. We also quantified the expression levels of the markers of glial cell activation i.e., GFAP in SN and spinal cord (SC) post-SN injury and the effects of BaBG on them. Further, to investigate the effect of BaBG axonal damage, we performed analyses involving NF-L-positive staining of SN. Moreover, we investigated the effect of BaBG on alterations in the neuronal morphology in the CCI model using Golgi-Cox staining. Additionally, we quantified myatrophy using hematoxylin and eosin staining in this model and evaluated the effects of BaBG on it. **Figure 6.1** illustrates the graphical representation depicting the schematic diagram outlining the proposed hypothesis concerning the molecular mechanism underlying the pathogenesis of NP in a rat model induced by CCI of SN and the effect of BaBG on them.

Hypothesis

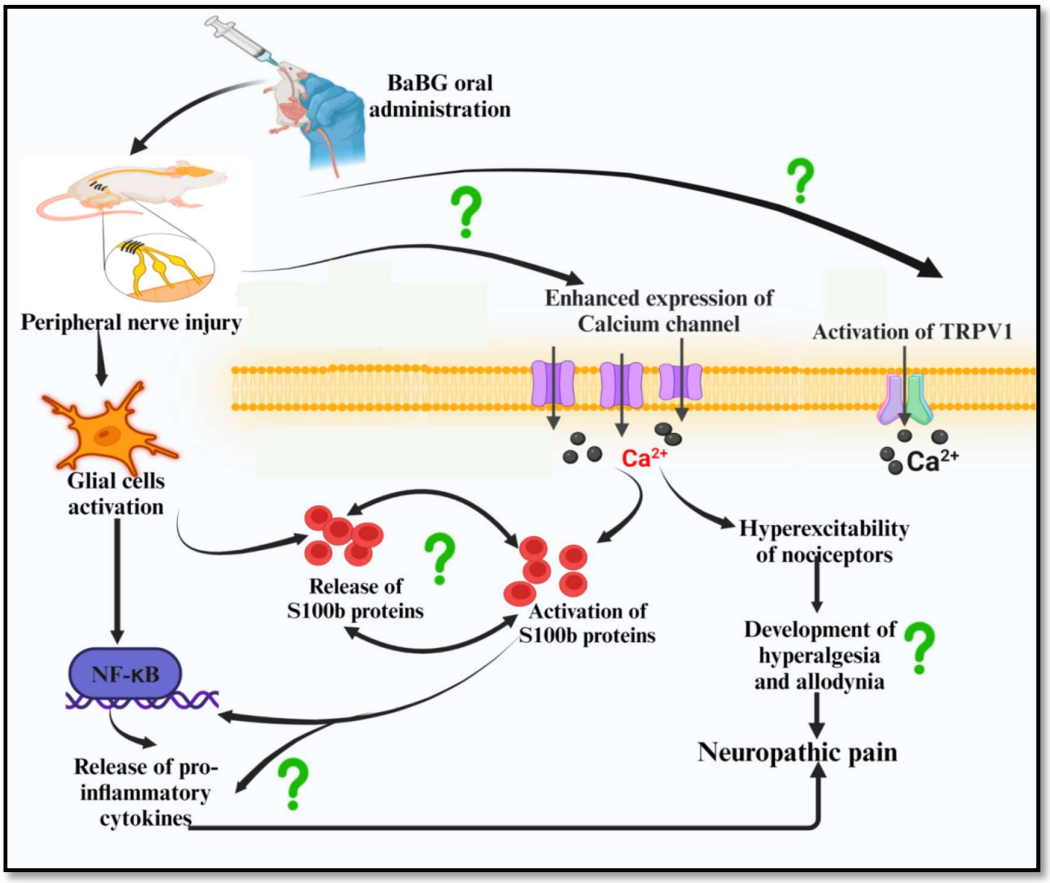

Figure 6.1 presents a graphical representation depicting the schematic diagram outlining the proposed hypothesis concerning the molecular mechanism underlying the pathogenesis of NP in a CCI-induced NP rat model. The injury to the sciatic nerve (SN) leads to central sensitization due to upregulation in the expression of calcium channels ($Ca_v2.2$) in the dorsal horn of the spinal cord (SC). Besides, there are also enhanced expression of heat-sensing TRPV1 channels in the SC. Enhanced expression of these channels increases the influx of calcium ions leading to hyper excitation of the nociceptive neurons and the development of NP phenotypes. In addition, the glial cells get activated post-CCI leading to an increase in the release of calcium-binding proteins i.e., S100b that further triggers the release of pro-inflammatory cytokines and contributes to the progression of NP. Barium-doped bioactive glass (BaBG) leaches barium ions from its framework after coming in contact with the physiological fluid. BaBG, due to its calcium-modulating effects may alleviate sensory and motor deficits observed in the CCI-induced NP in rats. It may also prevent the activation of calcium-binding protein i.e., S100b, reduce neuroinflammation, and concurrently cause axonal repair and remodeling; hence may have disease-modifying effects.

6.1. Materials and methods

6.1.1. Materials

The molecular biology kits and reagents used in the qPCR experiment include TRI reagent & DEPC that was sourced from Sigma. The revert aid cDNA synthesis kit (Thermo Scientific), TURBO DNA-freeTM (Ambion), TURBO DNA-free™ Kit (Invitrogen), Maxima SYBR Green/ ROX qPCR master mix 2X and primers (Eurofins Genomics India), Prestained protein MW marker (Puregene) and 100bp DNA marker (MBI Fermentas), 6X DNA loading buffer (Thermo Scientific), and RNAase cocktail (Invitrogen) was used in this study. All the primer sequences used (**detailed in Table 6.1**) were sourced from Eurofins Scientific. Triton X-100, Dabco, 3-aminopropyltriethoxysilane, and formaldehyde were acquired from Sigma, USA. Tween-20 was purchased from Merck and DAPI was obtained from SRL. Fura2 AM was purchased from ChemCruz. For the study, the ELISA kits used were from Krishgen Biosystems. The primary antibodies used in the experiment are GFAP (No.: ab7260, Abcam), S100b (No. E-AB-60087; Elabscience Biotechnology Co., Ltd., USA), NF-L (No. CST-2837T; Cell Signaling Technology), and Iba1 (No. 019-19741; FUJIFILM Wako Chemicals U.S.A.). The secondary antibodies used are goat anti-rabbit IgG FITC (ab6717; Abcam) and goat anti-rabbit IgG TRITC (ab6718, Abcam). The Luxol fast blue stain (CAS No. 1328-51-4) was obtained from Himedia, India.

6.1.2. Experimental animals and their ethical statement

The experiment used adult male Wistar albino rats weighing 200 ± 20 g, which were procured from the Central Animal House, IMS-BHU, Varanasi, India. Before commencing the experiment, the rats had one week of acclimatization at a consistent temperature of 25±1°C, with a 12-hour cycle of light and darkness. The experimental

animals were provided with *ad libitum* supply to a regular laboratory feed and water during the entire course of the trial. The rats were kept in cages measuring 430 x 270 x 150 mm and filled with corn cob bedding. Every possible attempt was made to decrease the quantity of animals utilized throughout the experiment. The experiments were conducted following the guidelines of the Committee for the Control and Supervision of Experiments on Animals (CCSEA), Government of India and "Care and Use of Experimental Animals" (Vol.1, 2nd ed., 1993, and Vol.2, 1984) guidelines of National Institute of Health, U.S.A. The experimental protocol for the present study evaluating the pharmacological effects of BaBG for the treatment of NP was approved by the Institutional Animal Ethical Committee (IIT(BHU)/IAEC/2022/037). Similarly, for performing the *ex vivo* electrophysiological assessment of calcium channel blocking effects of BaBG was approved by the Institutional Animal Ethical Committee (IIT(BHU)/IAEC/2023/029).

6.1.3. *Ex vivo* electrophysiological assessment of calcium channel blocking effects of BaBG

6.1.3.1. Preparation of physiological fluid (PF)

To prepare the PF, 112 mM NaCl, 2mM KCl, 2 mM NaH_2PO_4, and 1 mM $CaCl_2$ were used. All the salts were weighed and dissolved in distilled water and the pH was adjusted to 7.4. The solution was then stored at room temperature before usage. Before using the PF for the experiment, BaBG and 45S5 were weighed (1.5 mg/mL) and incubated in it for 3 days at room temperature. Then the PF was filtered and the supernatant was utilized in the *ex vivo* electrophysiological study.

6.1.3.2. *Ex vivo* electrophysiological assessment

All the Wistar rats were weighed and randomly allocated to seven experimental groups namely: (A) In the PF, (B) In the PF containing Pregabalin, (C) In the PF containing

BaBG, (D) In the PF containing $BaCl_2$, (E) In the PF containing 45S5, (F) In the PF containing reduced calcium ions and BaBG, and (G) In the PF containing BaBG and Pregabalin. Each group had four animals (n=4 rats/ group). The rats were anesthetized using thiopental sodium (50 mg/kg, *i.p.*) and euthanized. The sciatic nerve (SN) was isolated and care was taken not to touch the nerve with any metal forceps as metals touching the tissue may conduct electrical charges and alter the physiological activity of it. The isolated nerve was then stabilized in physiological fluid (PF) at 37 °C for 30 min. Then SN was placed on the nerve chamber (iWorx NCB-401) and stimulated at 1V. The compound nerve action potential (CAP) was generated was recorded using aniWorx214-two channel data recorder connected to the laboratory desktop PC running LabScribe (version 4.014000) (Medler 2022) as illustrated in **Figure 6.2**. Immediately after recoding, the SN was transferred back to the fresh PF to prevent drying out and to recover from the treatment effect.

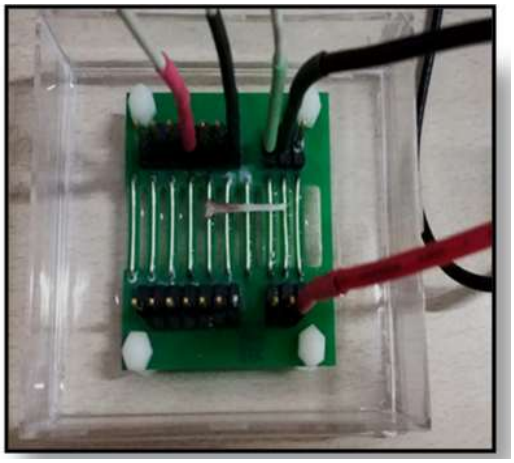

Figure 6.2. Schematic representation of the Plexiglas nerve bath chamber nerve apparatus with the ground, stimulating, and recording electrode used in the experiment. The isolated sciatic nerve (SN) is placed over the platform of the nerve chamber in the presence of physiological fluid containing the test compounds is stimulated and the compound nerve action potential (CAP) generated is recorded.

6.1.4. Chronic constriction injury (CCI) model of Neuropathic pain

The NP was induced in the rats by CCI of the sciatic nerve (Bennett 1993) as mentioned in **Chapter 5**. The experimental animals were anaesthetized intra-peritoneally using ketamine (80 mg/kg) and xylazine (10 mg/kg). Once under anesthesia, the rats were put on a 37 °C thermo-regulated heating surface. An incision parallel to the femur was made after shaving and sterilizing the right leg skin. The sciatic nerve was exposed by a gluteal muscle incision. Around 10 mm of the sciatic nerve proximal to the trifurcation was freed from the surrounding connective tissue and four loose ligatures (silk 4/0; Ethicon, USA) were tied with a gap of 1 mm around the nerve. The constriction of the sciatic nerve while tying the ligatures was done till a brief twitch was observed to prevent obstruction of the epineural blood flow. After suturing the muscle with 6/0 reabsorbable suture, the animals were kept under observation. Iodine solution was applied before and after incision suturing to reduce local infection.

6.1.5. Experimental design for pharmacological evaluation of BaBG for the treatment of NP

Before establishing the experimental protocol, a G*power analysis was performed to identify the appropriate sample size. This analysis aimed to ensure that the type I and II errors are maintained below the acceptable level, as proposed by Cohen (Cohen 1988). All the Wistar rats were weighed and a randomized allocation was employed to assign animals to the seven experimental groups: Control, CCI, CCI + BaBG (1 mg/kg *p.o*), CCI + BaBG (5 mg/kg *p.o*), CCI + BaBG (10 mg/kg *p.o*), CCI + 45S5 (10 mg/kg *p.o*), and CCI + Pregabalin (30 mg/kg *p.o*). Each group had twelve animals (n=12 rats/ group). The experiment was performed for a period of 28 days. NP was induced by CCI

of SN and the behavioral assessments (hot-plate test, Randall Selitto test, acetone drop test, cotton swab test, rota rod test, sciatic functional index (SFI), and BBB (Basso, Beattie, and Bresnahan) test) were performed before the surgery (D-0) and on day 7, 14, 21, and 28 post-surgery to access NP phenotypes developed. Dosing was started from D-14 after the NP phenotypes were stabilized following CCI and continued up to D-28 (**Figure 6.3**). Following this, the anaesthetized animals were sacrificed by decapitation (3% v/v isoflurane inhalation; R620 veterinary anesthesia machine, RWD life science, San Diego, USA). The SN of the ipsilateral side of the leg and SC were harvested. The dissected tissues were immediately stored at -80 °C until further research. The tissues collected were processed for neurochemical and molecular analysis.

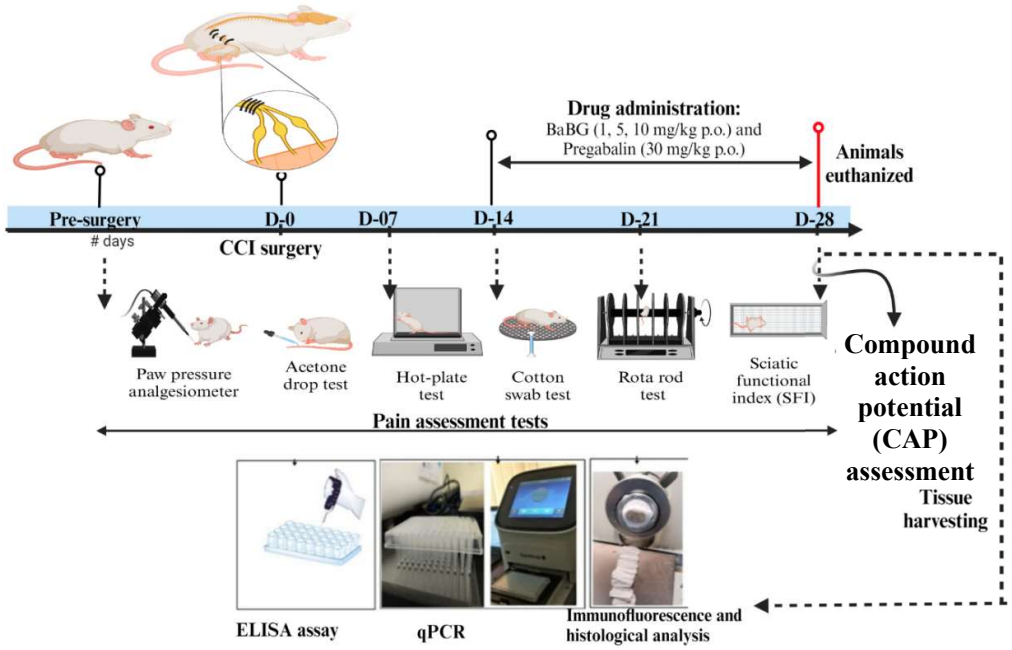

Figure 6.3: Schematic representation of the experimental protocol followed for the pharmacological evaluation of BaBG for the treatment of NP in rat CCI model.

6.1.6. Behavioral analysis:

The experimental animals were acclimatized to the testing environment before the baseline behavioral testing. The development of NP phenotypes was assessed before CCI surgery and on days 7, 14, 21, and 28 post-surgery.

6.1.6.1. Thermal hyperalgesia (hot-plate test)

The assessment of heat hyperalgesia in rats after surgery was conducted using Eddy's hot plate (Orchid Scientific, India) (Khangura, Bali et al. 2017). The plate's surface was warmed and the temperature was consistently maintained at 52.5 ± 0.5 °C. Next, the animals were placed on the hot plate and the time it took for them to exhibit the nocifensive withdrawal reaction, such as elevating and licking the rear paw of the injured side was recorded as nociceptive threshold. In order to prevent burn injuries to the animals, a cut-off period of 20 seconds was upheld.

6.1.6.2. Cold allodynia (acetone drop test)

The acetone drop test was used to assess the emergence of pain sensation in response to non-noxious stimuli (cool) following CCI surgery. During this experiment, the rats were initially adapted to a room with a mesh floor for 20 minutes. Subsequently, a volume of 100 µL of acetone was applied to the upper surface of the hind paw of the wounded leg. The frequent withdrawal, licking, biting, or flinching of the paw indicates the presence of cold allodynia, which is caused by the evaporation of acetone. The entire time of the withdrawal of the paw in the air, until it was placed back on the surface of the mess, was measured in seconds (Khangura, Bali et al. 2017).

6.1.6.3. Mechanical hyperalgesia (Randall Selitto test)

The Randall Selitto test-based digital paw pressure analgesiometer (Orchid Scientific, India) evaluated hyperalgesia to mechanical stimulation by measuring the mechanical nociceptive threshold to animal paw pressure. This test applies an increasing mechanical force focally to the dorsal surface of the impaired leg's hind paw using the pressure applicator until a withdrawal nociceptive response is detected. Pressure at which rats vocalized or displayed painful responses (flinching or withdrawal of paw or leg following stimulation) was recorded as the endpoint. The mean of three values interpreted to force in grams was the nociceptive threshold (Randall 1957, Ferrari, Rey et al. 2022).

6.1.6.4. Dynamic mechanical allodynia (Cotton swab test)

The cotton swab test in rats identified the development of dynamic mechanical allodynia after the induction of neuropathic pain by CCI (Field, Bramwell et al. 1999). Prior to the test session, the animals were acclimated to the Plexiglas chamber with mesh flooring to reduce their usual movements throughout the test duration. Next, a cotton swab was used to gently touch the planter portion of the ipsilateral hind paw of rats. The time it took for the paw to withdraw was measured, with a maximum time limit of 15 seconds.

6.1.6.5. Rota rod

The rotarod test is used to evaluate the motor coordination skills of rats after surgery (Prajapati, Garabadu et al. 2017). The animals under investigation are subjected to a two-day training period on the Rota rod (IKON instruments, India) at a minimum speed of 5 rpm. This is done to ensure that they achieve a consistent baseline performance.

Subsequently, in the testing phase, the rotational speed of the rod was elevated to 15 revolutions per minute. The animals' entire duration on the rod was recorded, with a maximum time limit of 300 seconds.

6.1.6.6. Sciatic functional index (SFI):

The SFI (sciatic functional index) was determined using the walking track analysis method, where the animals were required to travel on a straight track of 8.3 X 43 cm darkened at one end (de Medinaceli, Freed et al. 1982, Komirishetty, Areti et al. 2017). The SFI value is a scale that spans from 0 to -100. A number of 0 indicates normal functioning, while a value of -100 indicates complete impairment. Following two or three attempts on the track, the rats were trained to go directly to the dimly lit end without engaging in any exploration of the route. Subsequently, a sheet of white paper was positioned on the pathway, and the rear paws of the rats were immersed in distinct color solutions, with the uninjured left paw in green and the wounded right paw in red. Subsequently, the animal was positioned at the beginning of the track and given permission to traverse the paper. The ink on the paper had dried, and subsequent measurements were taken:

Print length (PL): The length of one foot print of normal (NPL) and experimental side (EPL).

Total spreading (TS): The linear distance between the center of first toe print and the center of fifth toe print of normal (NTS) and experimental side (ETS).

Distance between intermediary toes (IT): The linear distance between the center of second toe print and the center of fourth toe print of normal (NIT) and experimental side (EIT).

The SFI was calculated using the following formula:

SFI = -38.8(EPL-NPL)/NPL + 109.5(ETS-NTS)/NTS + 13.3(EIT-NIT)/NIT – 8.8

6.1.6.7. BBB (Basso, Beattie, and Bresnahan) locomotor test:

The BBB test is typically used to evaluate the decline in motor function following CCI of the SN in rats (Basso, Beattie et al. 1995). A trained observer, who was unaware of the experiment, assigns a score ranging from 0 to 21 based on the animal's movement. A score of 0 was assigned in the absence of any voluntary movement, whereas a score of 21 was given when the rats exhibited typical limb movement. Typically, a score of 14 is assigned to an animal that demonstrates full limb coordination. In this experiment, the animals being studied are placed in an open circular cage and monitored for 4 minutes and awarded scores accordingly.

6.1.7. Electrophysiological measurement of action potential

The rats were anesthetized and their core temperature was maintained at 37 °C using a homeothermic blanket device (Harvard, UK). Then the fur covering the hind limbs was shaved when the animals were already under analgesia. To ensure that no pathogens were introduced during the process, the shaved surface of the ipsilateral limb was cleaned with 70 % ethanol. Further, to ensure optimal conductivity and minimize transfer resistance while placing the electrodes, the contact gel was applied. The motor nerve conduction velocity (MNCV) was assessed by applying a single stimulus to the SN (proximal to the sciatic notch) and the tibial nerve (distal to the ankle) using bipolar needle electrodes with a diameter of 26 1/2 gauge and an intensity of 3 volts (Saini, HS et al. 2007). In the study, the Power Lab 8sp system (AD Instruments, Australia) was utilized to measure the Motor Nerve Conduction Velocity (MNCV). The CMAP (compound motor action potential) generated was recorded and its amplitude which is

a measure of the magnitude between the highest positive and lowest negative points of the CMAP signal, expressed in millivolts (mV) was calculated. Latencies were measured in each case from the initial onset of the CMAP. Further, MNCV was calculated using the formula:

$$\text{MNCV} = \frac{\text{Distance between sciatic and tibial nerve stimulation point}}{\text{Sciatic M wave latency} - \text{Tibial M wave latency}}$$

After completion of measurement, the rats were transferred to a separate cage until it has regained sufficient consciousness.

6.1.8. Electromyogram (EMG) recordings

During the CMAP recording, the EMG from the gastrocnemius muscle was measured in response to cold stimuli while the animal was regaining consciousness in order to measure changes in nocifensive reflexes. This was done by dropping acetone on the upper surface of the hind paw of the wounded leg (Monassi, Bandler et al. 2003). The raw EMG signals were then subjected to fast Fourier transformation (FFT; Chart v 4 software, AD Instrument), using 10 s epochs.

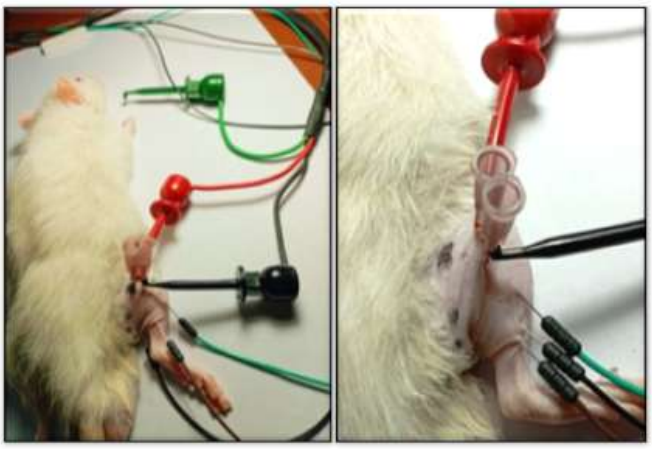

Figure 6.4: Representative images of the EMG recording from the gastrocnemius muscle in response to the cold-stimulus-evoked allodynia in the experimental rats.

6.1.9. Gastrocnemius muscle mass assessment:

The injury of the sciatic nerve leads to atrophy of the largest muscle supplied by it i.e., the gastrocnemius muscle which was assessed using the weight ratio of the gastrocnemius muscle 14 days after the surgery (Mohammadi, Amini et al. 2012). After the animals were euthanized, the gastrocnemius muscle was dissected from the contralateral and ipsilateral sides and weighed when wet using an electronic balance.

6.1.10. Real Time quantitative PCR

Quantitative Real-Time PCR (qRT-PCR) was performed as per the protocol mentioned in section 5.1.7 to assess the expression of the following genes at the mRNA level: NF-κB, Cav2.2, TRPV1 GFAP, and S100b. For normalization, β-actin was used as a constitutive type control.

Table 6.1: Primer sequences used for qRTPCR

Name	Primer sequences
NF-κB	F- 5'- GCGTTTCCGTTACAAGTGCGAGG -3'
	R - 5'- CCCCAGGAATACTGCCTGCAGAG -3'
Cav2.2	F- 5'- AGGCCAGACATGAAGACACACA -3'
	R - 5'- TTGCCTTCCTTGCTTGAGTCCT -3'
TRPV1	F- 5'- GAATGACACCATCGCTCTGC -3'
	R - 5'- AAGAGGGTCACCAGCGTCAT -3'
GFAP	F- 5'- AAGAAAACCGCATCACCATTCC -3'
	R - 5'- CCTTAATGACCTCGCCATCCC -3'
S100b	F- 5'- GAGAGAGGGTGACAAGCACAA -3'
	R - 5'- GGCCATAAACTCCTGGAAGTC -3'
β-actin	F- 5'-AGACTTCGAGCAAGAGATGGC -3'
	R-5'GATTCCATACCCAGGAAGGAAGG -3'

6.1.11. Assessment of S100b, TNF-α, IL-6, and IL-10 protein level in sciatic nerve and spinal cord

S100b (No: KLR1360, Krishgen Biosystems), TNF-α (No: KB3145, Krishgen Biosystems), IL-6 ELISA Kit (No: KB3068, Krishgen Biosystems), and IL-10 (No: E-EL-R0016, Elabscience, USA) were used in this study to quantitatively assess the protein levels in SN and SC following the manufacturer's instructions. The protein concentrations were determined using the Bradford method (Bradford 1976).

6.1.12. Immunofluoresence analysis

The expression of GFAP, S100b, and NF-L in the SN and SC were performed according to the protocol mention in section 5.1.9. (Prajapati, Ahmed et al. 2024).

6.1.13. Golgi –Cox Staining

Golgi-Cox staining is a neurohistological technique employed to examine the cytoarchitecture of the nervous system. In this study, we followed the protocol mention in section 5.1.10.

6.1.14. Measurement of intracellular calcium level

The intracellular calcium level was measured in the SN and SC following the protocol mentioned in section 5.1.11 (Malgaroli, Vallar et al. 1987).

6.1.15. Histological analysis of gastrocnemius muscle

The gastrocnemius muscle was fixed in a 10% buffered formalin solution which was sliced (5 μm) using the cryostat. Then the finely sliced sections were stained with hematoxylin followed by counterstaining with eosin. Then the tissue sections were dehydrated with a graded series of alcohol and mounted with dibutyl phthalate xylene

(DPX). The slides were then observed under the microscope (Olympus, Japan) for any structural abnormalities (Majumdar and Krishnamurthy 2022).

6.1.16. Histological analysis of sciatic nerve (SN) using luxol fast blue staining

The luxol fast blue stain is used to stain the myelinated axons and Nissil substance to identify the damage caused to the neuronal structure post-CCI of SN. The SN was fixed in a 10 % buffered formalin solution and sliced (5 µm) using cryostat. Then the tissue slices were hydrated in distilled water followed by incubation in the luxol fast blue stain solution for 2 h at 60 °C as per the manufacturer's instructions (ab150675; Abcam). The slides were rinsed thoroughly in distilled water and dipped in lithium carbonate solution for 20 sec. Subsequently, the tissue sections were treated with alcohol to remove the excess stain followed by rinsing it using water. The slides were then incubated in cresol echt violet for 3 min and rinsed quickly. Then the tissue sections were dehydrated with a graded series of alcohol and mounted with dibutyl phthalate xylene (DPX).The slides were then observed under the microscope (Olympus, Japan) for any structural abnormalities (Nazeri, Derakhshan et al. 2022).

6.1.17. *In silico* docking of S100b proteins with metal ions (Ca^{2+} and Ba^{2+})

6.1.17.1. Preparation of Ligand and Protein

The MIB2 website, namely the Metal Ion-Binding site prediction and docking server, contains information regarding the presence of calcium and barium metal ions (Lu, Chen et al. 2022). The website may be accessed via http://combio.life.nctu.edu.tw/MIB2/.The rat S100b protein was acquired from the RCSB Protein Data Bank (https://www.rcsb.org/search) with PDB ID: 1XYD. The ligands and proteins were prepared using Chimera version 1.15, which can be downloaded from https://www.cgl.ucsf.edu/chimera/download.html.

6.1.17.2. Analysis and Visualization

Chimera version 1.15 is utilized for the examination and graphical representation of docking outcomes. Visualization is employed to elucidate the interaction between ligands and receptor protein residues, which manifests as the interaction of amino acids and the bond distance between ligands and receptor protein residues.

6.1.18. Statistical analysis

The data has been represented as Mean ± SD and the statistical analysis was conducted using GraphPad Prism 8. The CAP recorded during the *ex vivo* electrophysiological study was analyzed using one-way ANOVA followed by a Tukey multiple. The behavioral tests, including the hot-plate test, acetone drop test, Randall Selitto test, cotton swab test, rota rod test, BBB score, and SFI, were statistically assessed using a two-way ANOVA followed by a Bonferroni post-hoc test. The changes in intracellular calcium and pro-inflammatory cytokines levels after the BaBG treatment were examined using one-way ANOVA followed by Tukey multiple comparison post-hoc tests. Statistical significance was determined when the P value was less than 0.05 in the in entire data analysis.

6.2. Results and Discussion

6.2.1. Effect of calcium channel blocking (CCB) properties of BaBG in the *ex vivo* setup

NP following nerve damage is characterized by the upregulation in the voltage-gated calcium channel (VGCC) leading to maladaptive changes in the pain axis (Luo, Chaplan et al. 2001),resulting in elevated intracellular calcium ion concentration $(Ca^{2+})_i$. This is a key factor in the progression of NP as it enhances the excitability of neurons

due to the abnormal release of neurotransmitters that trigger pain-inducing downstream cascades; hence, facilitating additional calcium release, thereby worsening the painful symptoms (Cui, Wu et al. 2021). As a result, CCBs are used clinically for the management of NP symptoms (Alles, Cain et al. 2020). Similarly, in our investigation, we examined the CCB potential of BaBG using an *ex vivo* isolated SN setup. This setup was stimulated to generate CAP, as shown in **Figure 6.5**. Upon stimulation of the SN stabilized in PF, we observed the production of a CAP (**Figure 6.5A**). PF includes all the necessary ions (Na^+, Ca^{2+}, and K^+) that are involved in the various stages of action potential generation and transmission. Nevertheless, when the SN was submerged in the CCB solution, specifically pregabalin, there was an instantaneous and notable block in CAP generation (**Figure 6.5B**). This indicates that calcium is crucial for the onset and propagation of action potential. Further, **Figure 6.5C** illustrates the effect of BaBG on the CAP of the isolated SN. It is evident that when the SN is stimulated, a CAP is generated. However, the repolarization phase of the CAP was prolonged, indicating that BaBG impeded the transmission of CAP. We sought to determine if the observed effects of BaBG as observed in **Figure 6.5C** are attributable to the barium or other ions that have been released from the BaBG framework into the PF. Therefore, we have conducted stimulation on the SN that has been stabilized using barium salt, specifically $BaCl_2$. **Figure 6.5D** demonstrates that the presence of $BaCl_2$ resulted in the total absence of CAP formation. Hence, the observed effects in case of BaBG as represented in **Figure 6.5C** can be attributed to the combination of ions released from the BaBG network into the PF, which aids in the production of CAP but decelerate its rate of transmission and in case of NP, hypersensitivity of nociceptors is observed (Cahill, Holdridge et al. 2022). Further, research has indicated that complete blocking of

calcium channels as observed in case of organic CCBs has a greater number of negative consequences compared to partial blockers as organic CCBs exhibits physical interaction with the calcium channel and blocks the calcium-conducting pathway located in the central cavity of the channel (Tang, Gamal El-Din et al. 2016). This strong physical interaction with the calcium channel produces adverse effects like increased risk of atrial fibrillation (Moore, Straube et al. 2009, Park, Hunter et al. 2023) as seen in case of gabapentinoids. However, the inorganic compounds are most likely to have physiological interactions that modulate the potential difference across the neuronal membrane and impart its action.

Furthermore, we stimulated the SN after immersing it in a 45S5 solution that includes all ions present in BaBG, except for barium, as depicted in **Figure 6.5D**. It was noted that the generation and propagation of CAP were similar to that observed in the PF (**Figure 6.5A**), with the exception for a detected overshoot in the CAP. The rise in the amplitude of the CAP can be attributed to the release of Ca^{2+} from 45S5, resulting in an overall elevation in the extracellular fluid (ECM) concentration of Ca^{2+}. Previous reports have indicated that an excessive amount of Ca^{2+} in the ECM triggers an increase in the amplitude of the CAP, resulting in a “calcium spike” (Walsh Jr and Singer 1980).

Moreover, the CAP was measured in the presence of PF containing lower levels of calcium ions and BaBG, as shown in **Figure 6.5E**. We noticed an immediate depolarization phase caused by the presence of Na^{+} in PF and the dissolution fluid of BaBG. This was followed by an overshoot in CAP, known as the "barium spike" and then a prolonged repolarization phase. Supporting our observation, it has been reported that Ba^{2+} can substitute for Ca^{2+} (Walsh Jr and Singer 1980). Additionally, at the last phase of depolarization when the calcium channel opens, Ba^{2+} enters because it has

greater permeability for voltage-dependent calcium channels compared to Ca^{2+} (Hagiwara and Byerly 1981, Satoh, Kubota et al. 1987). Consequently, the action potential experiences a decreased rate of repolarization, potentially caused by its impact on the Ca^{2+}-activated K^{+} current (Vassort 1975). A prior study also demonstrated that the presence of Ba^{2+} in the extracellular fluid resulted in an extended action potential plateau observed in the growth cone of a regenerated axon in lamprey along with the concentration-dependent elongation in the spike (Macvicar's and Llinas 1985). Moreover, when BaBG in the PF was used alongside the CCB (pregabalin), the generation of CAP failed (**Figure 6.5G**). This confirms that the observed effects of BaBG in the *ex vivo* electrophysiological assessment are mediated through the calcium channel. Further, under NP conditions, there are reports of a reduction in the threshold required to elicit an action potential, resulting in hypersensitivity (Djouhri, Fang et al. 2012). Since, we observed that BaBG has the capacity to extend the repolarization phase of the produced CAP, thereby causing a delay in the propagation of the action potential. Hence, it has the potential to be used as a therapeutic strategy for NP treatment.

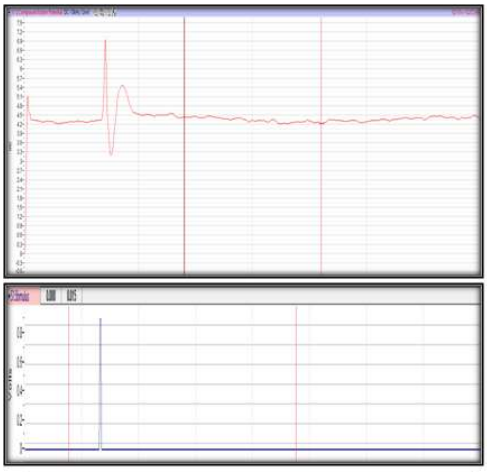

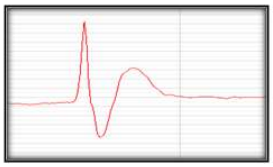

(A) In the PF

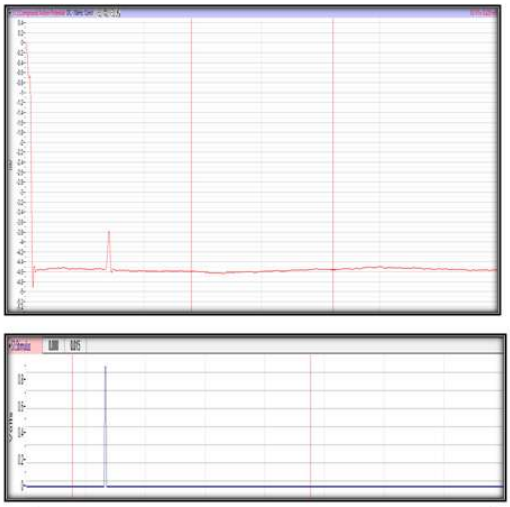

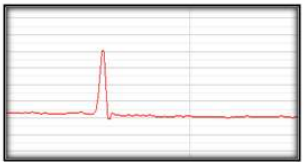

(B) In the PF containing Pregabalin

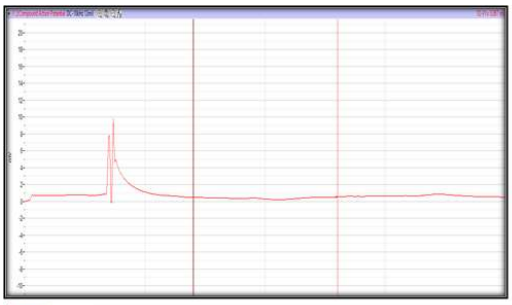

(C) In the PF containing BaBG

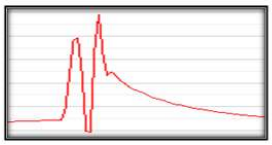

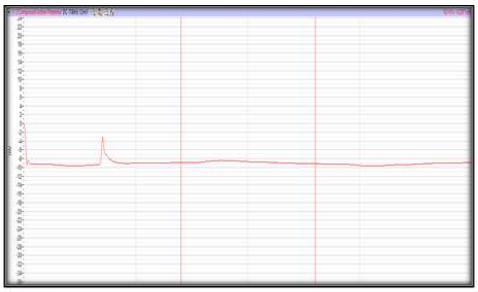

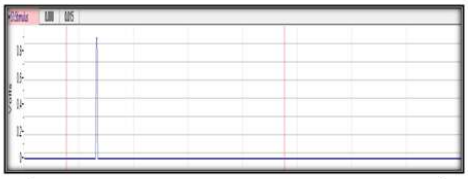

(D) In the PF containing $BaCl_2$

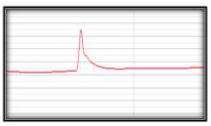

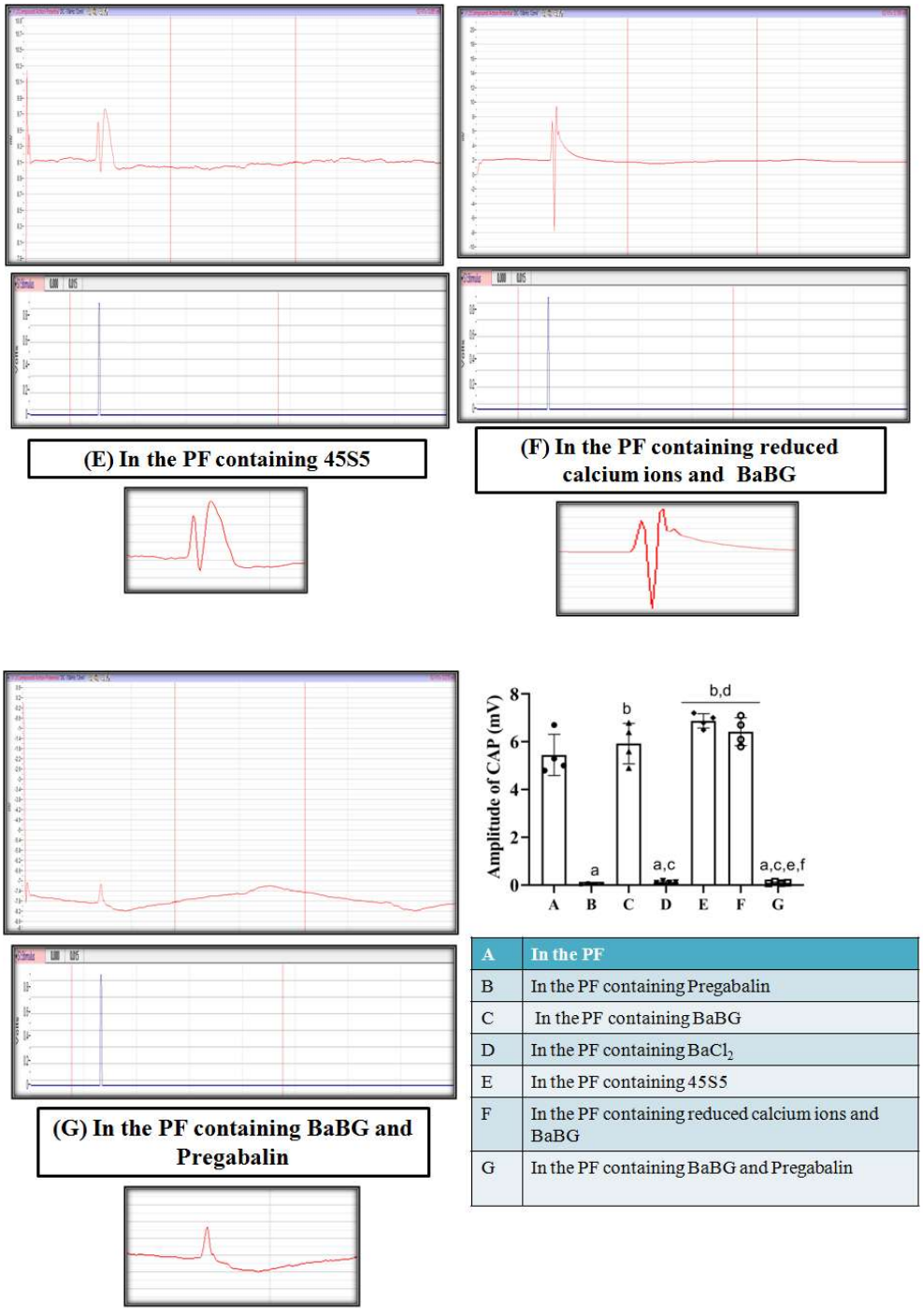

A	In the PF
B	In the PF containing Pregabalin
C	In the PF containing BaBG
D	In the PF containing $BaCl_2$
E	In the PF containing 45S5
F	In the PF containing reduced calcium ions and BaBG
G	In the PF containing BaBG and Pregabalin

Figure 6.5: Effect of BaBG on the generation of CAP. All values are mean ± SD (n=4). $^{a}P<0.05$, $^{b}P<0.05$, $^{c}P<0.05$, $^{d}P<0.05$, $^{e}P<0.05$, and $^{f}P<0.05$ compared to groups i.e., in the PF, in the PF containing Pregabalin, in the PF containing BaBG, in the PF containing $BaCl_2$, in the PF containing 45S5, in the PF containing reduced calcium ions and BaBG, and in the PF containing BaBG and Pregabalin respectively. (One-way ANOVA followed by Tukey's post hoc test).

6.2.2. Effect of BaBG on mechanical /thermal hyperalgesia and allodynia

The heightened hypersensitivity to non-noxious thermal and mechanical stimuli is an instructive trait observed clinically and preclinically in NP conditions (Jensen and Finnerup 2014, Edhi, Heijmans et al. 2020). Consequently, we used Randall Selitto and Eddy's hot-plate test in order to assess the efficacy of BaBG in reducing the severity of mechanical and thermal hyperalgesia respectively. In this study, after the CCI surgery, we observed the development of mechanical and thermal hyperalgesia as evident from a decrease in the threshold of withstand pressure (TWP) applied on the dorsal part of the paw and the paw withdrawal latency (PWL) in nerve-injured rats in response to thermal stimuli that started from day 7 and was maximum on day 14 (**Figure 6.6A and B**). The TWP and PWL of the ipsilateral side of CCI decreased to 61.48 ± 9.06 g and 5.16 ± 1.56 sec respectively compared to baseline 128.47 ± 14.38 g and 16.83 ± 1.26 sec respectively, suggesting the development of sensory hypersensitivity at the end of experimental protocol. Several research groups have also reported that CCI of SN can cause prolonged allodynia and hyperalgesia, as well as spontaneous pain behaviors (Edhi, Heijmans et al. 2020). Notably, there were no significant changes in the PWL and TWP of the contralateral paw compared to pre-CCI. Statistical analysis by two-way ANOVA exhibited differences in the ipsilateral paw mechanical withdrawal threshold and PWL after the treatment with BaBG among the groups ([$F(6, 385) = 203.5$; $p < 0.05$] and [$F(6, 385) = 205.8$; $p < 0.05$] respectively), time periods ([$F(4, 385) = 520.4$; $p < 0.05$] and [$F(4, 385) = 466.4$; $p < 0.05$] respectively) and the interaction between group and time ([$F(24, 385) = 25.42$; $p < 0.05$] and [$F(24, 385) = 25.20$; $p < 0.05$] respectively). Post hoc analysis revealed that all the doses (1, 5, and 10 mg/kg) of BaBG significantly improved the CCI-induced decrease in PWL and TWP. However, the effect

of BaBG at the doses of 5 and 10 mg/kg was more significant compared to BaBG 1 mg/kg and the onset of action was observed on day 21 and it continued till day 28 in a dose-dependent manner. Further, 45S5 (10 mg/kg) did not have significant effects in improving PWL and TWP compared to BaBG as shown in **Figure 6.6**. The ability of BaBG to mitigate the hyperalgesia to mechanical and thermal stimulus developed post-injury to the peripheral nerve may be due to its calcium channel blocking potential as observed in **Figure 6.5**. In support of our observation, previously, studies have confirmed that excessive upregulation of accessory units of VGCC contributes to the development of NP phenotypes after peripheral axonal injury due to excessive influx of Ca^{2+} that increases the excitability of primary afferent neurons (Luo, Chaplan et al. 2001).

Moreover, BaBG also attenuated the dynamic mechanical and cold allodynia in a dose-dependent manner during the acetone spray and cotton swab test respectively as shown in **Figure 6.6(C and D)**. Statistical analysis using repeated measures of two-way ANOVA revealed significant differences in paw withdrawal duration (PWD) and paw withdrawal latency in cotton swab test among the different groups ([$F(6, 385) = 200.7$, $p < 0.05$] and [$F(6, 385) = 264.0$, $p < 0.05$] respectively), as well as over time ([$F(4, 385) = 512.9$, $p < 0.05$] and [$F(4, 385) = 608.0$, $p < 0.05$] respectively). Additionally, an interaction between group and time was observed ([$F(24, 385) = 23.02$, $p < 0.05$] and [$F(24, 385) = 22.67$, $p < 0.05$] respectively). The contralateral paw did not exhibit significant differences according to post hoc analysis (data not shown). Post hoc analysis represented that all the doses of BaBG ameliorated CCI-induced increase in cold and dynamic mechanical allodynia on D-28 of experimental protocol. On the other hand, 45S5 (10 mg/kg) attenuated cold and dynamic mechanical allodynia; however,

the effects seen were not as significant as BaBG. Taken together, our results suggest that BaBG reversed all the core sensory phenotypes of NP in a dose-dependent manner.

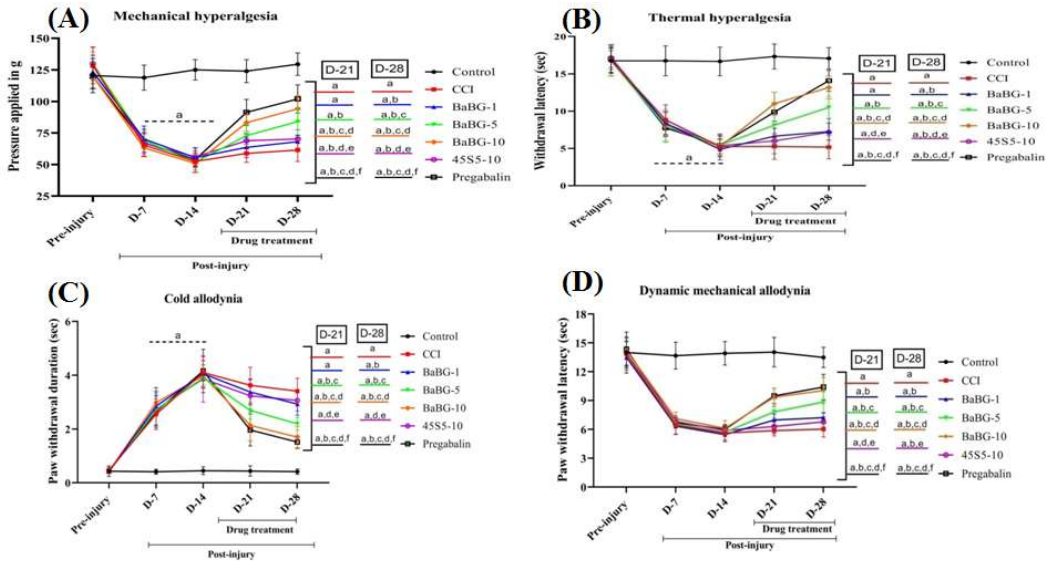

Figure 6.6: Effect of BaBG on (A) mechanical hyperalgesia, (B) thermal hyperalgesia, (C) cold allodynia, and (D) dynamic mechanical allodynia. All values are in mean ± SD (n=12 rats/ group). $^{a}p<0.05$, $^{b}p<0.05$, $^{c}p<0.05$, $^{d}p<0.05$, $^{e}p<0.05$, and $^{f}p<0.05$ compared to control, CCI, BaBG-1, BaBG-5, BaBG-10, and 45S5-10 respectively (Two-way ANOVA followed by Bonferroni post-hoc test)

6.2.3. Effect of BaBG on the CCI-induced alterations in motor functions

The SN innervates various muscles in the lower limb that are essential for plantar flexion of the foot at the ankle joint and flexion of the leg at the knee joint. Therefore, injury to SN in the CCI model of NP leads to the development of motor incoordination and gait abnormalities (Ahmad, Subhan et al. 2021). The gait and weight bearing of rodents can be examined as an alternative measure of nociception and are commonly regarded as indicators of non-evoked or stimulus-independent 'pain'. Gait analysis in freely ambulating rodents is employed to investigate alterations in limb motion and sensorimotor impairment. In order to assess the extent of functional recovery after the BaBG treatment, we conducted a walking track test and the SFI was calculated on a

weekly basis. In the walking track analysis paradigm, the SFI decreased with CCI injury [$F(6,385) = 902.1$; $p<0.05$]. These changes were observed with respect to time [$F(4,385) = 2009$; $p<0.05$] (**Figure 6.7A**). Further, there was a significant interaction between groups and time [$F(24,385) = 83.65$; $p<0.05$] in this paradigm. Post hoc analysis represented that, all the doses of BaBG (1, 5, and 10 mg/kg) ameliorated CCI-induced decrease in SFI(-75.58 ± 6.33) on D-28. Further, the effect of BaBG on SFI at the dose of 5 and 10 mg/kg (-48.48 ± 8.13 and -25.91 ± 4.09 respectively) was more significant compared to the lowest dose of BaBG i.e., 1 mg/kg (-59.36 ± 4.23). Further, 45S5 (10 mg/kg) also improved the CCI-induced motor deficits but was not as potent as BaBG of the same dose and its effects were comparable to the lowest dose of BaBG. Moreover, the impairment in the motor coordination post-injury to the peripheral nerve was confirmed by the BBB score of the CCI group which had reduced to 4.91 ± 0.99 on day-28 compared to baseline 19.66 ± 0.65. However, BaBG (10 mg/kg) significantly improved the BBB score to 17.01 ± 0.72 after two weeks of treatment compared to the nerve-injured rats.

Furthermore, the effect of BaBG on neuromuscular coordination was also assessed using the rotarod tests. Statistical analysis using repeated measures of two-way ANOVA revealed significant differences in rotarod retention time (RRT) observed among the different groups [$F (6, 385) = 117.4$, $p < 0.05$], over time [$F(4, 385) = 335.0$, $p < 0.05$] and interaction between group and time [$F (24, 385) = 18.65$, $p < 0.05$] as shown in **Figure 6.7C**. The CCI group exhibited a decline in RRT starting from D-7 compared to the control group, indicating the presence of motor deficits similar to the observed limping gait in patients (Drăghici, Văcăraș et al. 2023). We observed that RRT for the CCI rats has reduced significantly to 65.05 ± 8.14 seconds at the end of the experimental

protocol compared to baseline 112.16 ± 11.75 seconds. However, administration of BaBG (1, 5, 10 mg/kg) significantly restored motor function, resulting in an increase in RRT compared to the CCI group as observed on day 28 (i.e. after 14 days of treatment) of the study protocol. These effects continued to increase progressively up to D-28. On day 28, no significant differences were observed between the higher dose-treated group and the pregabalin-treated group in terms of RRT. The highest dose of BaBG improved RRT to 103.11 ± 8.87 sec while the RRT in the moderate dose i.e., 5 mg/kg was increased to 87.93 ± 9.94. On the contrary, treatment with 45S5 (10 mg/kg) did not show any significant improvement in the motor deficits compared to CCI rats. Hence, it can be concluded that BaBG improved CCI-induced motor deficits in a dose-dependent manner.

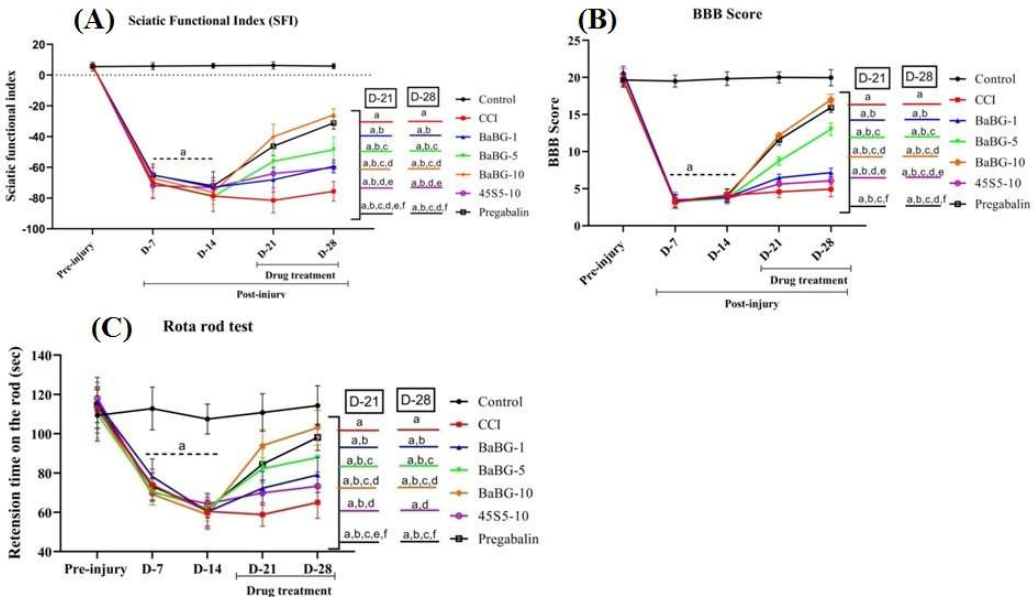

Figure 6.7: Effect of BaBG on (A) SFI, (B) BBB score, and (C) time spent on rota rod. All values are in mean ± SD (n=12 rats/ group). [a]p<0.05, [b]p<0.05, [c]p<0.05, [d]p<0.05, [e]p<0.05, and [f]p<0.05 compared to control, CCI, BaBG-1, BaBG-5, BaBG-10, and 45S5-10 respectively (Two-way ANOVA followed by Bonferroni post-hoc test)

6.2.4. Effect of BaBG on the mRNA expression of TRPV1 and Ca_V 2.2 along with the intracellular calcium level $(Ca^{2+})_i$ in the SN and SC post-CCI

To analyze the effects of BaBG on the $Ca_V2.2$ expression in the SN and SC and to identify the significant differences among the groups, statistical analysis by one-way ANOVA was employed ([$F(6,27) = 64.77$; $p<0.05$] and ([$F(6,27) = 132.4$; $p<0.05$] respectively). Post-hoc analysis revealed a significant increase in the mRNA expression of $Ca_V2.2$ in both SN and SC following CCI compared to control rats (**Figure 6.8 iC and D**). The over-expression of VGCC, specifically Ca_V 2.2, in nociceptors, has also been reported previously that leads to an influx of cations, which causes depolarization of the corresponding neuronal ending. The depolarization triggers the formation of an action potential that carries the nociceptive signal from A-δ and C nerve fibers into the central nervous system (CNS) (Saegusa, Matsuda et al. 2002, Antunes, Campos et al. 2023). Further, the upregulated Ca_V 2.2 post-injury has been directly linked to the development of behavioral hypersensitivity and synaptic plasticity during the NP conditions (Luo, Calcutt et al. 2002). In addition, tactile allodynia, which is commonly observed in patients with NP and animal models of NP, has been associated with an increase in the auxiliary unit of VGCC (Luo, Calcutt et al. 2002). However, BaBG treatment exhibited a substantial decrease in the expression of $Ca_V2.2$ in SN and SC in a dose-dependent manner. It was observed that there was an attenuation of 47.90 and 39.63 % in the $Ca_V2.2$ expression in SN and SC respectively post-BaBG treatment at the highest dose compared to the CCI group. On the contrary, 45S5 at a dose of 10 mg/kg could not reverse the CCI-induced enhanced expression of $Ca_V2.2$ in SN and SC. Therefore, our findings suggest that the addition of barium to the 45S5 framework

imparts these observed molecular effects in the CCI-induced NP model leading to attenuation of the sensory hypersensitivity.

Voltage-dependent calcium channels have a multifaceted role in nociception, as they allow Ca^{2+} to enter the cell. These ions contribute to membrane depolarization and also act as a second messenger, triggering a wide range of cellular processes including the release of neurotransmitters such as glutamate, substance P, and calcitonin gene-related peptides and increasing the chronicity of pain (Smith, Cabot et al. 2002, Takasusuki and Yaksh 2011). In our study, one-way ANOVA revealed a difference in $(Ca^{2+})_i$ level post-treatment with BaBG in SN [$F(6,27)= 14.14$; $p<0.05$] and SC [$F(6,27)= 61.79$; $p<0.05$] among the groups. Tukey's post-hoc test showed a significant increase in $(Ca^{2+})_i$ level in both SN and SC following CCI compared to the control group. However, this elevation was mitigated by BaBG after 14 days of treatment in a dose-dependent manner. Dose-dependent effects of BaBG on the calcium channel suggest its specific calcium-modulating pharmacological action with minimum off-target interactions. Besides, the changes observed in $(Ca^{2+})_i$ level in the BaBG-treated group can be due to the calcium channel modulating effects observed in **Figure 6.5**. Interestingly, unlike BaBG, treatment with 45S5 did not significantly alter the elevated $(Ca^{2+})_i$ level in SN and SC post-injury to the peripheral nerve compared to CCI rats ($P > 0.05$) (as shown in **Figure 6.8ii A and B**).

Thermal sensitivity is a frequently observed symptom in both clinical and preclinical reports following nerve damage (Chen, Willcockson et al. 2009, Huang, Lu et al. 2020). The transient receptor potential channel (TRPV1) is known to be linked to the development of increased sensitivity to heat (thermal hyperalgesia) (Huang, Lu et al. 2020). Therefore, we have examined the effect of BaBG on the expression of TRPV1

in the SN and SC following CCI injury (**Figure 6.8iA and B**). One-way ANOVA represented significant alteration in TRPV1 mRNA expression in the SC and SC among the groups ([F(6,27) = 84.08; p<0.05] and ([F(6,27) = 108.1; p<0.05] respectively on D-28. Post-hoc analysis demonstrated a substantial increase in the TRPV1 expression in both SN and SC compared to the control group. Treatment with various doses (1, 5, and 10 mg/kg) of BaBG effectively mitigated the expression of TRPV1 compared to CCI rats. In addition, the effect of BaBG at the dose of 5 and 10 mg/kg was more pronounced compared to the lowest dose of BaBG i.e., 1 mg/kg. Nevertheless, when given at a dose of 10 mg/kg, the administration of 45S5 exhibited mild pharmacological activity in the CCI model in alleviating heat sensitivity that was comparable to the lowest dose of BaBG (1 mg/kg). The results of our study demonstrate that the inclusion of barium enhances the effectiveness of 45S5 in reversing NP phenotypes. This is achieved by regulating calcium ions through calcium channels and altering the expression of TRPV1, which is responsible for aberrant temperature perceptions in NP.

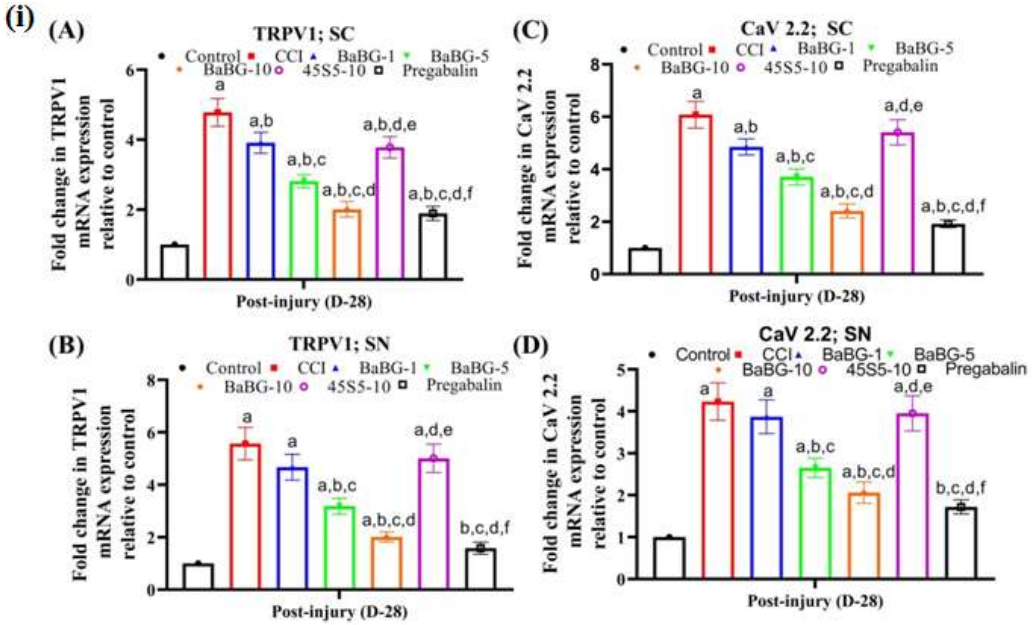

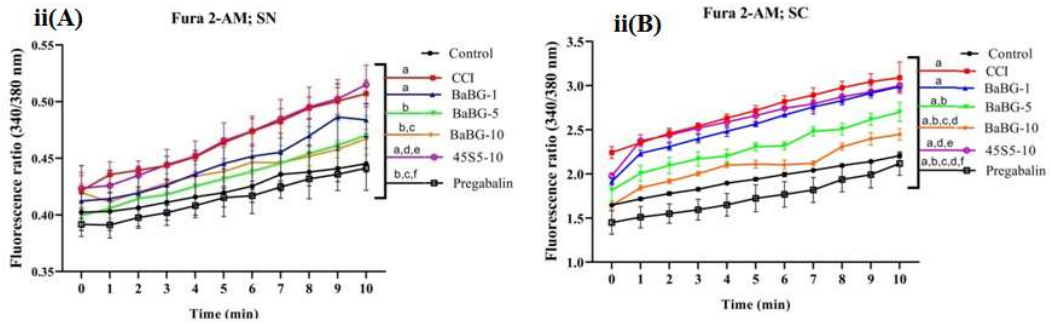

Figure 6.8: Effect of BaBG on the (i) mRNA expression of TRPV1 and Cav2.2, and on (ii) the intracellular calcium level in the SN and SC. (ii). All values are in mean ± SD (n=4 / group). $^{a}p<0.05$, $^{b}p<0.05$, $^{c}p<0.05$, $^{d}p<0.05$, $^{e}p<0.05$, and $^{f}p<0.05$ compared to control, CCI, BaBG-1, BaBG-5, BaBG-10, and 45S5-10 respectively. (One-way ANOVA followed by Tukey's multiple comparison post-hoc test)

6.2.5. Effect of BaBG on the expression of S100b in SN and SC

Chapter 5 has demonstrated a direct relationship between the S100b level and the onset and progression of NP phenotypes. Additionally, the specific S100b inhibitor, pentamidine, has been found to alleviate sensory and motor impairments in the CCI model of NP. Therefore, we have evaluated the effects of BaBG on the expression of calcium-binding protein i.e., S100b in the SN and SC. One-way ANOVA revealed a significant difference in the fluorescence intensity of S100b expression among the groups in SN ([$F(6,20) = 30.16$; $p<0.05$]) and SC ([$F(6,20) = 11.78$; $p<0.05$]) compared to the control group as shown in **Figure 6.9 and 6.10** respectively. Post-hoc test showed a significant increase in the S100b protein expression following CCI injury in the SN and SC compared to the control rats. A similar trend was observed in the mRNA expression of S100b in the SN and SC post-injury to the peripheral nerve as shown in **Figure 6.13 (iB and iiB)**. These observations are consistent with the clinical reports which showed an exaggerated response of S100b in traumatic injury (Lécuyer, Mercier et al. 2021). Similarly, previous studies found enhanced expression of S100b in chronic pain models in rodents (Celikbilek, Akyol et al. 2014). Interestingly, treatment with

different doses of BaBG significantly alleviated the CCI-induced increased S100b expression in a dose-dependent manner. In support of our observation, previous studies have demonstrated that the presence of Ba^{2+} prevented the secretion of S100b from the primary astrocyte culture (Vizuete, Hansen et al. 2019). However, 45S5 (10 mg/kg) did not produce a significant effect on the increased S100b level following CCI. Elevated levels of S100b reflect the activation of glial cells, which in turn stimulates inflammatory responses, hence contributing to the chronic nature of NP (Michetti, Di Sante et al. 2021). Nevertheless, our earlier investigation showed that the release of barium from BaBG exhibits anti-inflammatory properties in the LPS-induced neuroinflammation in the C6 cell line (Majumdar, Hira et al. 2021). Hence, the anti-inflammatory properties of BaBG may hinder the feedback process that triggers the continued release of S100b from the activated glial cells. In addition, after CCI injury, we saw a gradual rise in the intracellular calcium concentration $(Ca^{2+})i$, which subsequently led to an increase in the release and activation of the calcium-binding protein (S100b) as described in **Chapter 6.5**. Further, based on the observations in **Figures 6.5 and 6.8**, it can be inferred that BaBG has the ability to modulate calcium levels. Consequently, the decline in intracellular calcium concentration $(Ca^{2+})_i$ may have led to a reduction in the expression of S100b after BaBG treatment. However, pregabalin (30 mg/kg) did not have significant effects on the elevated S100b level following CCI injury compared to BaBG, thus highlighting the effectiveness of BaBG in the injury-induced glial cell activation that is involved in the pathophysiological process in chronic pain.

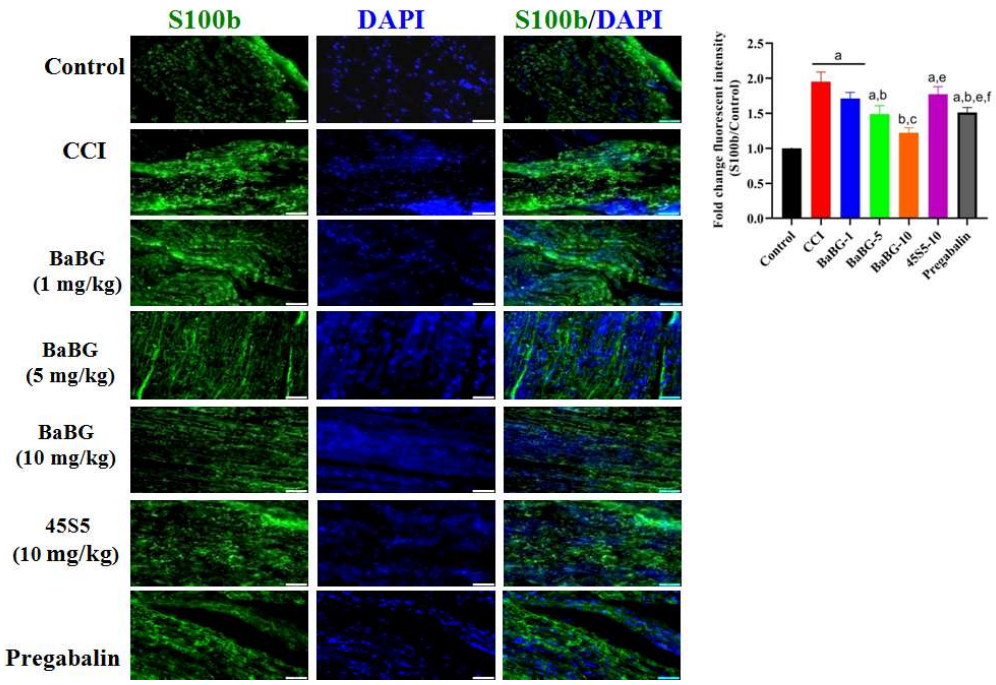

Figure 6.9: Effect of BaBG on S100b expression in the SN. Scale bar was set at 50 µM with 20X magnification. All values are in mean ± SD (n=3 rats/ group). [a]p<0.05, [b]p<0.05, [c]p<0.05, [d]p<0.05, [e]p<0.05, and [f]p<0.05 compared to control, CCI, BaBG-1, BaBG-5, BaBG-10, and 45S5-10 respectively. (One-way ANOVA followed by Tukey's multiple comparison post-hoc test)

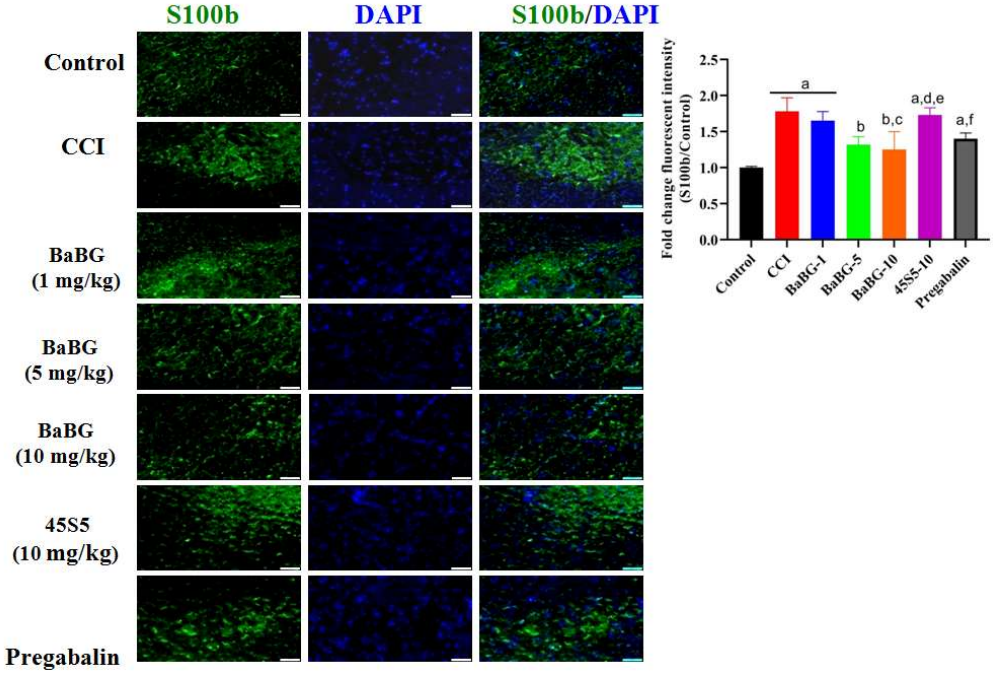

Figure 6.10: Effect of BaBG on S100b expression in the SC. Scale bar was set at 50 µM with 20X magnification. All values are in mean ± SD (n=3 rats/ group). [a]p<0.05, [b]p<0.05, [c]p<0.05, [d]p<0.05, [e]p<0.05, and [f]p<0.05 compared to control, CCI, BaBG-1, BaBG-5, BaBG-10, and

45S5-10 respectively. (One-way ANOVA followed by Tukey's multiple comparison post-hoc test)

6.2.6. Effect of BaBG on the CCI-induced astrocytes activation in SN and SC

In the present study, we have measured the GFAP expression in the SN and SC as an indicator of the astrocytes activation post-CCI of SN using an immunofluoresence assay. Statistical analysis using one-way ANOVA showed a significant difference in the fluorescence intensity of S100b expression among the groups in SN ($F(6,20) = 22.37$; $p<0.05$) and SC ($F(6,20) = 10.91$; $p<0.05$) compared to the control group, as depicted in **Figure 6.11 and 6.12**, respectively. The post-hoc test revealed a statistically significant rise in the expression of the GFAP protein after CCI injury in the SN and SC when compared to the control rats. A comparable pattern was noted in the mRNA levels of GFAP in the injured SN and SC following peripheral nerve damage, as depicted in **Figure 6.13 (iA and iiA)**. These data align with the preclinical reports in rodent models of chronic pain that show an amplified response of GFAP in cases of severe spinal nerve injury (Romero-Sandoval, Chai et al. 2008). The aberrant glial cell activation contributes to hypersensitivity and aids in the maintenance of hyperalgesia and allodynia in NP (Romero-Sandoval, Chai et al. 2008). In addition, prolonged activation of astroglia following neuronal injury is reported to be associated with the maintenance of a prolonged state of chronic neuroinflammation, contributing to the persistence of NP (Fan, Zhang et al. 2023). Treatment with BaBG alleviated these alterations significantly ($p < 0.05$) on D-28 of the experimental protocol in a dose-dependent manner. The effect of BaBG at the dosage of 5 and 10 mg/kg was more prominent in comparison to the lowest dosage of BaBG, which is 1 mg/kg. However, when administered at a dosage of 10 mg/kg, 45S5 showed slight pharmacological effects in

the CCI model by reducing the GFAP expression, which was similar to the lowest dosage of BaBG (1 mg/kg). Further, the highest dose of BaBG (10 mg/kg) was found to mitigate the CCI-induced increase in GFAP expression which was comparable to the pregabalin treated group ($p > 0.05$).

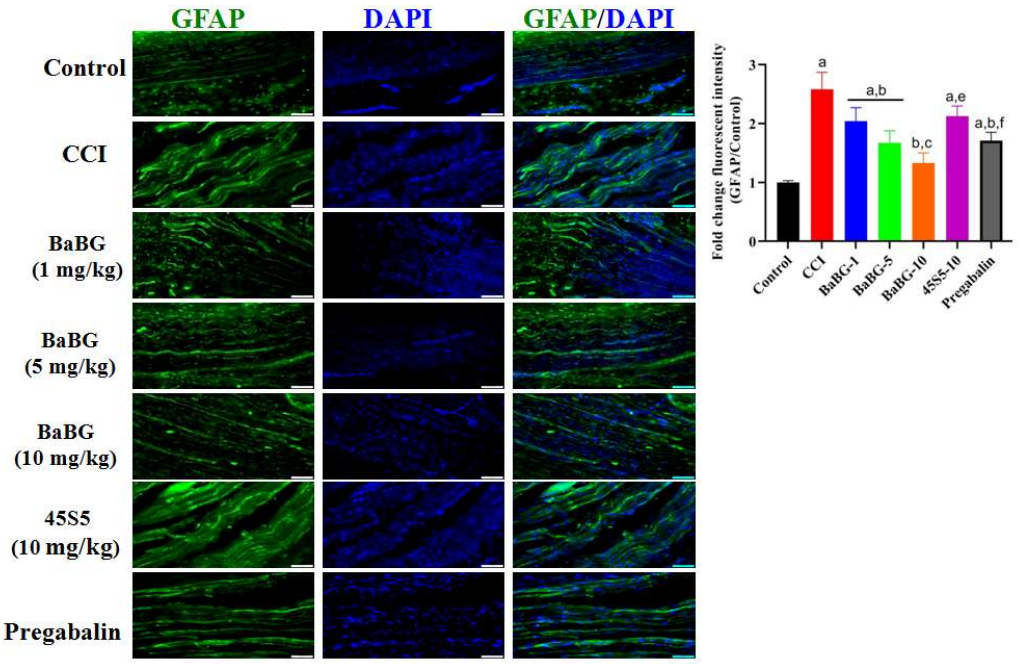

Figure 6.11: Effect of BaBG on GFAP expression in the SN. Scale bar was set at 50 µM with 20X magnification. All values are in mean ± SD (n=3 rats/ group). [a]p<0.05, [b]p<0.05, [c]p<0.05, [d]p<0.05, [e]p<0.05, and [f]p<0.05 compared to control, CCI, BaBG-1, BaBG-5, BaBG-10, and45S5-10 respectively. (One-way ANOVA followed by Tukey's multiple comparison post-hoc test)

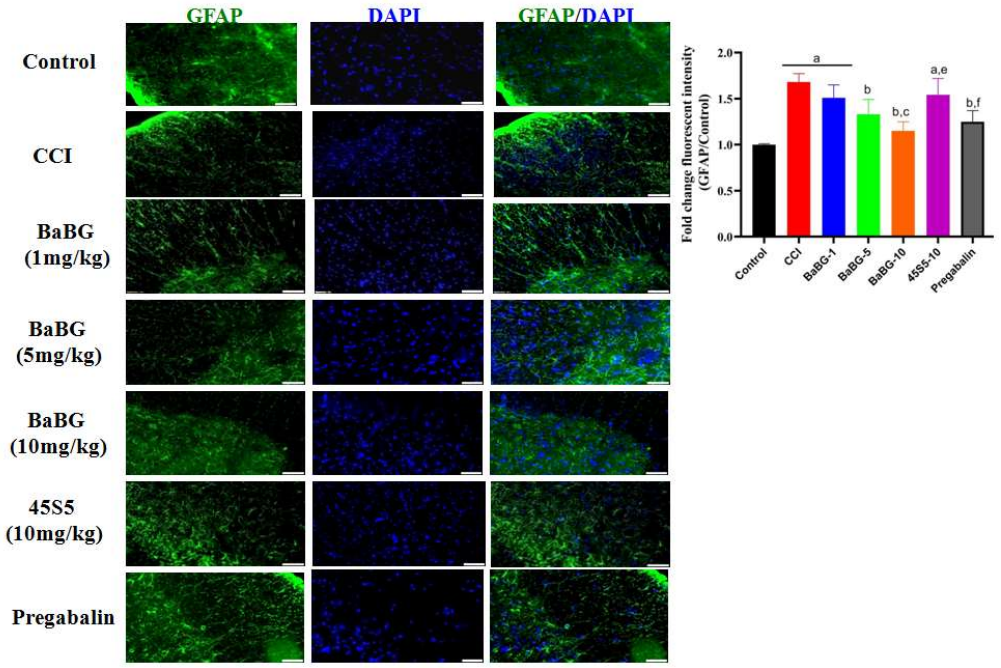

Figure 6.12: Effect of BaBG on GFAP expression in the SC. Scale bar was set at 50 µM with 20X magnification. All values are in mean ± SD (n=3 rats/ group). [a]p<0.05, [b]p<0.05, [c]p<0.05, [d]p<0.05, [e]p<0.05, and [f]p<0.05 compared to control, CCI, BaBG-1, BaBG-5, BaBG-10, and 45S5-10 respectively. (One-way ANOVA followed by Tukey's multiple comparison post-hoc test)

6.2.7. Effect of BaBG on the CCI-induced neuroinflammation

To investigate the effect of BaBG (1, 5, and 10 mg/kg) on CCI-induced neuroinflammation, we analyzed the levels of pro-inflammatory cytokines and investigated the underlying mechanisms. In the present study, one-way ANOVA showed that there were significant differences in pro-inflammatory cytokine i.e., TNF-α level in the SN and SC among the group ([F(6,27) = 77.85 p<0.05] and [F(6,27) = 57.60; p<0.05] respectively**)** as depicted in **Figure 6.14(B and E)**. Following the CCI, there were also notable variations in IL-6 levels among different groups in the SN and SC, as indicated by the statistical analysis ([F(6,27) = 19.19; p<0.05] and [F(6,27) = 20.35; p<0.05] respectively**),** illustrated in **Figure 6.14(A and D)**. Post hoc analysis revealed that there was a significant increase in the pro-inflammatory cytokines level

(TNF-α and IL-6) compared to the control rats. In the CCI group, the levels of TNF-α were elevated by 3.86-fold and 2.93-fold in the SN and SC, respectively compared to the control rats. Similarly, the levels of IL-6 in the disease group had increased by a factor of 1.84 and 2.12 in the SN and SC, respectively. Treatment with BaBG5 and 10 mg/kg significantly alleviated the CCI-induced alteration in TNF-α and IL-6. BaBG at the highest dose reduced the TNF-α 2.56-fold and 2.14-fold in SN and SC respectively compared to CCI rats. Likewise, IL-6 level was attenuated in the SN and SC by 1.62-fold and 1.74-fold respectively by the treatment with 10 mg/kg of BaBG. Nevertheless, the lowest dose of BaBG proved to be ineffective in this regard. The CCB used in the study i.e., Pregabalin (30 mg/kg) also elicited a reduction in the CCI-induced neuroinflammation but was not as effective as BaBG (10 mg/kg). Further, 45S5 (10 mg/kg) did not show any changes in the pro-inflammatory cytokine levels compared to the CCI group.

Moreover, the anti-inflammatory effect elicited by BaBG in the CCI model was clearly demonstrated by the significant increase in IL-10 levels in the SC and SN as shown in **Figure 6.14(C and F)**. Through the utilization of a one-way ANOVA analysis, notable changes were observed between various groups in terms of IL-10 protein level in the SN [$F(6, 27) = 35.65$; $p < 0.05$] and SC [$F(6, 27) = 39.93$; $p < 0.05$]. In rats following CCI, there was a substantial reduction in the levels of IL-10 protein in SN and SC by 1.95-fold and 1.99-fold respectively compared to the control group. However, BaBG exhibited a dose-dependent significant increase in the IL-10 level compared to CCI rats. These observations are consistent with our previous study where BaBG exhibited anti-inflammatory effects in the *in vitro* LPS-induced neuroinflammation model (Majumdar, Hira et al. 2021) as demonstrated in **Chapter 2**.

As we saw in **Chapter 5**, there was an aberrant rise in the intracellular calcium level in the SN and SC after the CCI, which augmented the levels of the calcium-binding protein, or S100b. In addition, there was neuroinflammation caused by injury, as indicated by the increased levels of pro-inflammatory cytokines (**Figure 6.14**). Further, in our study, there were significant differences in the mRNA gene expression of NF-κB among different groups as shown in **Figure 6.13(iC and iiC)**. One-way ANOVA revealed significant variations in NF-κB gene expression in SN and SC ([F (6, 27) = 17.09; $p < 0.05$] and [F (6, 27) = 27.20; $p < 0.05$] respectively). The post hoc test revealed that NF-κB mRNA expression had significantly elevated in the SN and SC of the CCI group compared to naïve rats. More precisely, there was a 3.18 and 3.27-fold rise in NF-κB expression in SN and SC respectively of CCI rats. Following an injury, there is glial activation that triggers the aberrant release of calcium-binding proteins (S100b) that interact with a range of cell surface receptors, including RAGE and toll-like receptors, by attaching to calcium ions and exposing its hydrophobic binding site (Singh and Ali 2022, Goswami, Anuradha et al. 2023). These events initiate a pro-inflammatory cascade through downstream signaling, which activates numerous transcription factors, including NF-κB (Yesudhas, Gosu et al. 2014). However, the treatment with BaBG effectively alleviated the notable increase in NF-κB ($p < 0.05$), a key regulator of inflammatory responses on D-28. In contrast, 45S5 (10 mg/kg) did not exhibit a significant effect on CCI-induced increase in NF-κB expression in SN and SC. This implies that the anti-inflammatory effects observed are due to the doping of barium into the 45S5 framework.

In addition, we conducted molecular docking experiments of the S100b protein with Ca^{2+} and Ba^{2+} ions using MIB2, as depicted in **Figure 6.15**. The calcium and barium

metal ions are depicted as bright yellow circles positioned within the bonded amino acid residues, as seen in **Figure 6.15 i and ii**, respectively. The 3D prediction model indicates that both Ca^{2+} and Ba^{2+} ions bind to the same active region on the EF-hand of the S100b protein in rats. Nevertheless, the affinity of Ba^{2+} for binding was determined to be greater than that of Ca^{2+}, as depicted in **Figure 15iii**. In addition, prior research has shown that the presence of Ba^{2+} inhibits the release of S100b from primary astrocyte cultures (Vizuete, Hansen et al. 2019). Consequently, the barium released from the BaBG tends to reduce the release of S100b from the activated glial cells following CCI, thereby mitigating the activation of pro-inflammatory pathways.

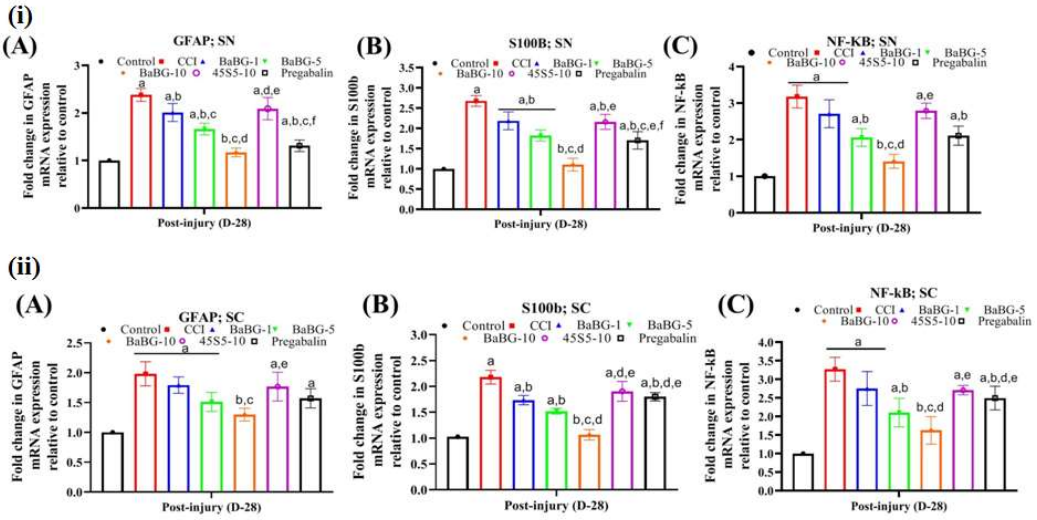

Figure 6.13: Effect of BaBG in the mRNA expression of GFAP, S100b, and NF-kB expression in the SN (i) and SC (ii). All values are in mean ± SD (n=4 / group). $^{a}p<0.05$, $^{b}p<0.05$, $^{c}p<0.05$, $^{d}p<0.05$, $^{e}p<0.05$, and $^{f}p<0.05$ compared to control, CCI, BaBG-1, BaBG-5, BaBG-10, and 45S5-10 respectively. (One-way ANOVA followed by Tukey's multiple comparison post-hoc test)

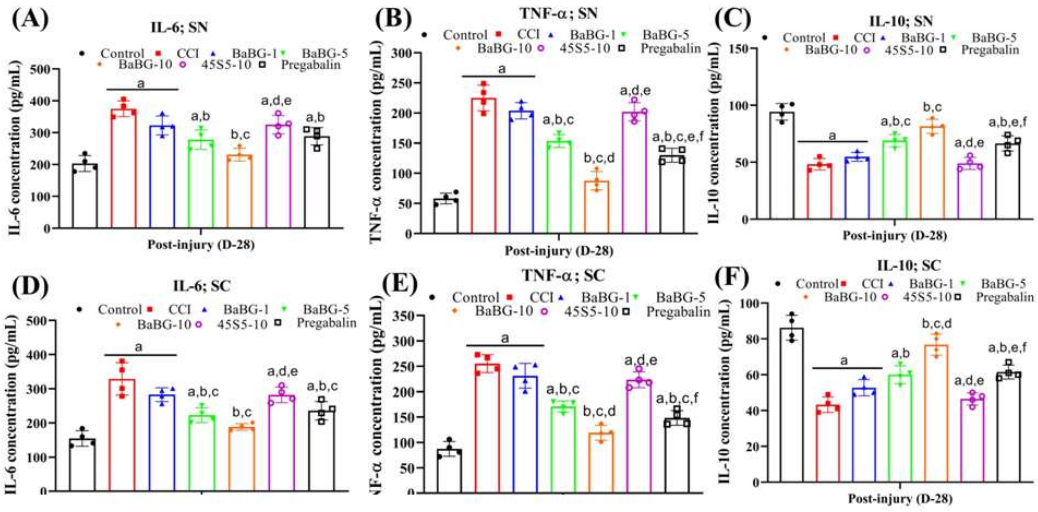

Figure 6.14: Effect of BaBG on TNF- α, IL-6, and IL-10 levels in the SN and SC. All values are in mean ± SD (n=4 / group). [a]p<0.05, [b]p<0.05, [c]p<0.05, [d]p<0.05, [e]p<0.05, and [f]p<0.05 compared to control, CCI, BaBG-1, BaBG-5, BaBG-10, and 45S5-10 respectively. (One-way ANOVA followed by Tukey's multiple comparison post-hoc test)

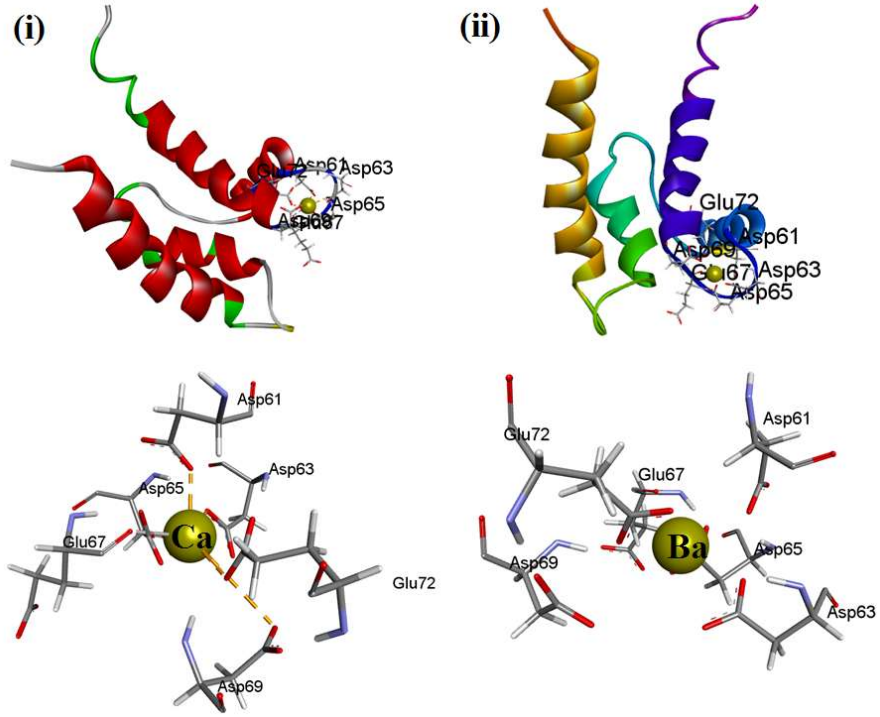

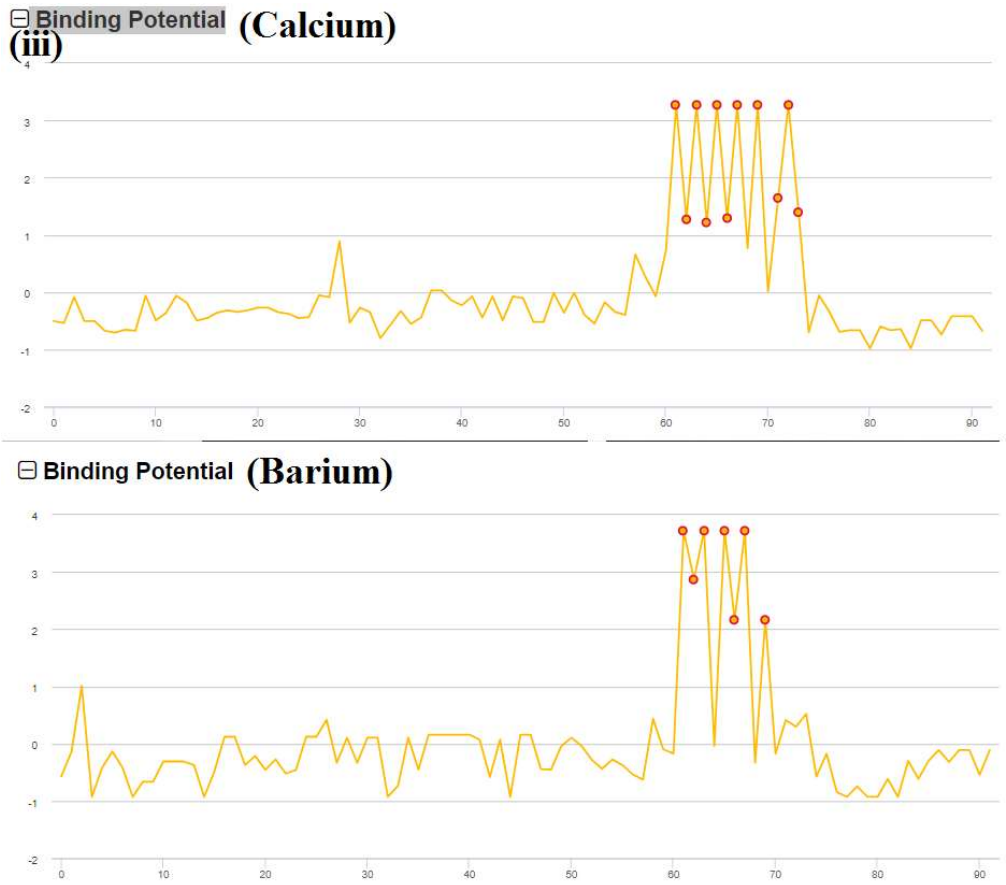

Figure 6.15: Molecular docking showing interaction of calcium (Ca^{2+}) and barium (Ba^{2+}) against S100b protein. 3D docking diagram of S100b bound to (i) Ca^{2+} and (ii) Ba^{2+}along with their (iii) binding potential.

6.2.8. Effect of BaBG on the neuronal morphology post-CCI injury

We examined the structure of neurons in the sections of the spinal cord after CCI injury, as depicted in **Figure 6.16**. The dendrites of neurons in the SC of CCI rats exhibited disintegration and retraction. After the peripheral nerve injury, the dendrites were fragmented and there was a decrease in the number of branches around the soma. However, treatment with BaBG as well as pregabalin led to dendrite arborization. In addition, we conducted a Sholl analysis on individual neurons, as shown in **Figure 6.17i**. The results showed that the intersections of dendrites with concentric circles at each radius were dramatically decreased in the injured rats. Statistical analysis using

the one-way ANOVA demonstrated significant differences in the total length of the dendrites [$F(4, 19) = 7.64$, $p < 0.05$, **Figure 6.17iiC**] among different experimental groups. Post-hoc analysis revealed that following treatment with BaBG (10 mg/kg) significantly increased the total length of the dendrites compared to the CCI group which had decreased significantly post-injury to the nerve. Furthermore, the dendritic arbors in the treatment group were longer and had more intersections at each radius compared with those in the CCI group, as determined by Sholl analysis (**Figure 6.17iiA and B**). The total length of the dendrites in the BaBG-treated group was 23.34 ± 6.58 μm significantly higher in comparison to the CCI group (9.89 ± 4.26 μm). Similarly, in the 45S5 and pregabalin-treated group, the total length of dendrites was found to be 19.91 ± 3.47 and 11.96 ± 6.39 μm respectively. The above results indicate that spinal neuronal dendrite arborization degenerated dramatically after CCI, but the degeneration was alleviated upon BaBG treatment. Similarly to our observations, it has been reported that when synaptic rewiring occurs, the remaining neurons try to rewire to make newer synaptic neural connections in order to repair and compensate for the loss of function (Tan, Stamboulian et al. 2008). The extent of functional recovery post-injury depends on the efficiency of neural circuit reconnection such as reactivating and reorganizing the intraspinal neuronal connections. Therefore, BaBG has the potential to rewire and reconnect which is essential for functional recovery.

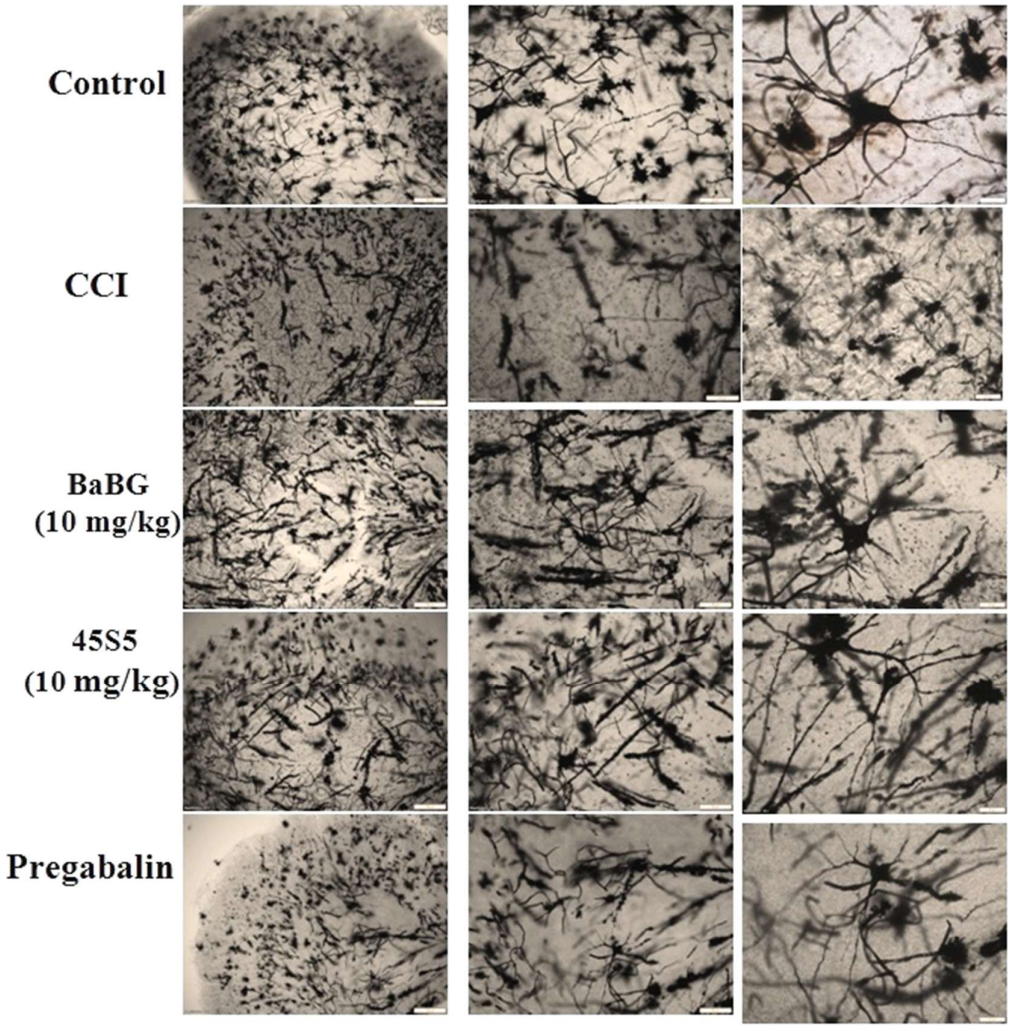

Figure 6.16: Representative images of Golgi-Cox impregnated SC slice of control, CCI, BaBG-10, 45S5-10 and pregabalin treated rats. Scale bar was set at 200, 100, and 50 μM with 4, 10, and 20X magnification.

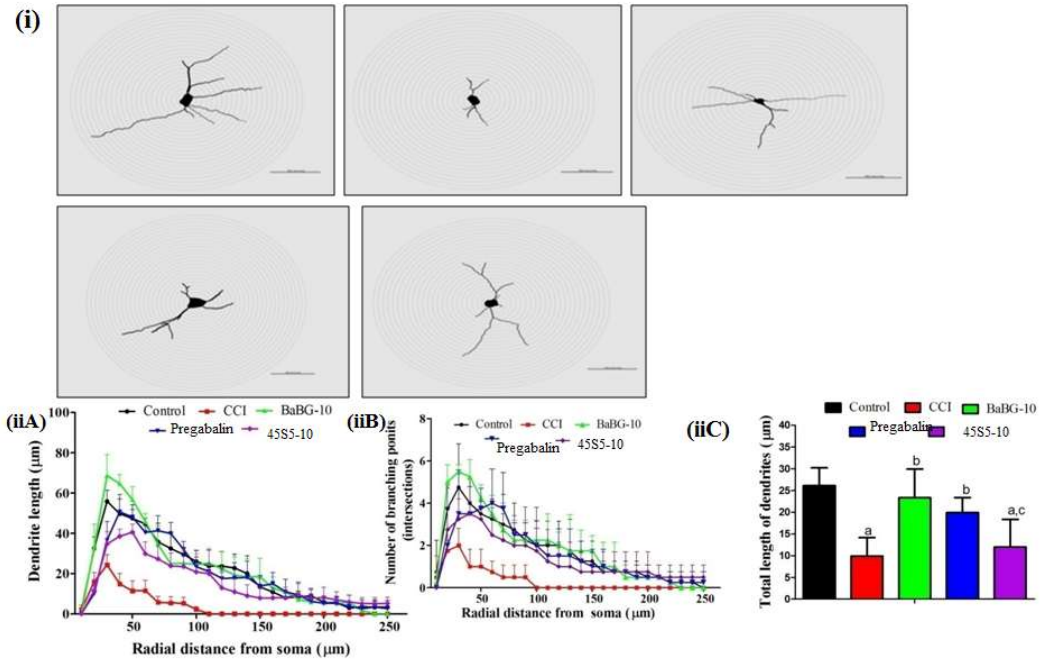

Figure 6.17: (i) Representative image of the camera Lucida drawing of neuron of SC which is superimposed over concentric circles using Sholl analysis. (ii) Effect of BaBG on (A), number of branching points (B) dendrite length across the soma, and (C) total length of dendrites. All values are in mean ± SD (n=4 / group). $^{a}p<0.05$, $^{b}p<0.05$, and $^{c}p<0.05$ compared to control, CCI, and BaBG-10 respectively. (One-way ANOVA followed by Tukey's post-hoc test)

6.2.9. Effect of BaBG on the CCI-induced axonal degeneration

Neurofilament light chain (NF-L) is a neuronal cytoplasmic protein particularly prominent in the large myelinated axons (Gaetani, Blennow et al. 2019). During the NP conditions, following the injury, there are reports of axonal degeneration leading to the fragmentation of NF-L, resulting in an increase in its concentration in the extracellular space and bloodstream(Widyadharma and Tedyanto 2022, Mortensen, Steffensen et al. 2023). Consequently, we have evaluated the effects of BaBG on the CCI-induced changes in NF-L expression in the SN as represented in **Figure 6.18**. One-way ANOVA followed by the post-hoc test indicated significant changes in the NF-L expression among the group [$F(6,20) = 28.19$; $p<0.05$]. Post-hoc test revealed a significant decrease in the fold change fluorescent intensity of NF-L in the SN of the CCI group

compared to the control rats. The control group exhibited alignment in NF-L, however after the CCI; NF-L was shown to be fragmented and scrambled, indicating axonal degeneration, as depicted in **Figure 6.18**. Following injury, the axon undergoes degeneration, resulting in the loss of myelin proteins that surround the axon in layers (**Figure 6.19**). This loss of myelin proteins leads to a decrease in the conduction velocity of the action potential, as seen in **Figure 6.21**. However, following the treatment with BaBG, the rats had increased NF-L expression in the SN in comparison to the CCI group, suggesting axonal repair. In contrast, the administration of pregabalin at a dosage of 30 mg/kg was found to be less efficacious in reversing the CCI-induced axonal damage than the barium-doped biomaterial (BaBG). Additionally, we also noted that there was no significant difference in the NF-L expression between the 45S5 (10 mg/kg) treated group and the CCI group. Thus, these findings confirm that BaBG possesses the axonal repair ability, leading to observable functional restoration during the pain behavioral assessment tests.

Further, the morphometric assessment by Luxol Fast Blue (LFB) tissue staining enabled the characterization of the effect of BaBG in terms of alterations in myelin sheath thickness caused by CCI of SN. The histological examination of the specimens revealed a normal SN appearance in the control group with a regular distribution of myelin that is stacked as long and neat columns surrounded by the basement membrane (**Figure 6.19**, control). However, as anticipated, the CCI group had an irregular distribution of nerve fibers that were thinly myelinated (**Figure 6.19**, CCI – black arrows) with a high degree of myelin vacuolation, suggesting axonal atrophy (**Figure 6.19**, CCI –red star). In contrast, animals treated with BaBG exhibited a significant and dose-dependent restoration of myelin in their nerves. This was evident from the increased number of

nerve fibers that were enveloped by a greater amount of myelin, in comparison to the CCI group.

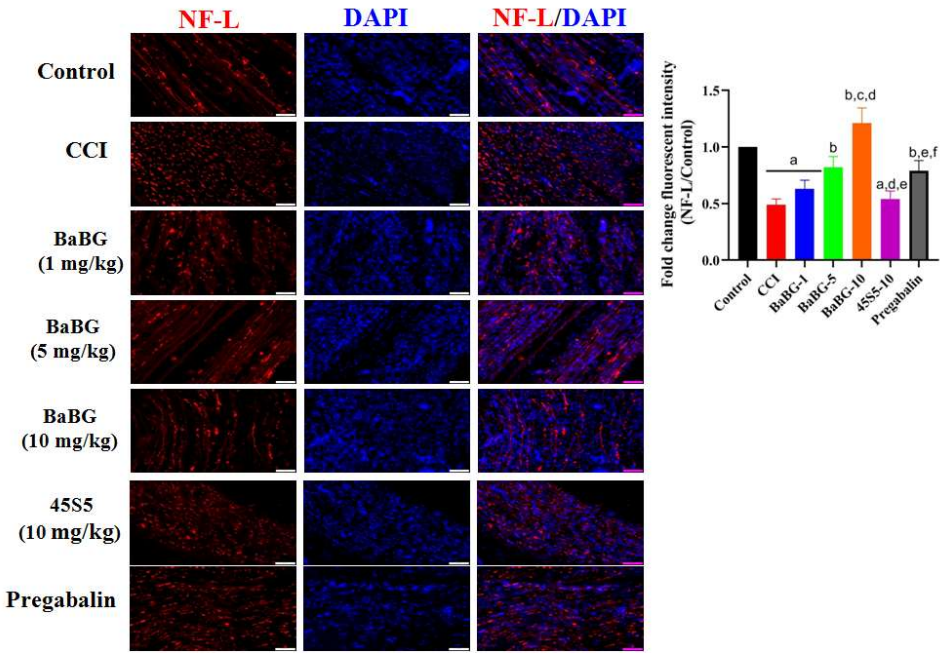

Figure 6.18: Effect of BaBG on NF-L expression in the SN. Scale bar was set at 50 µM with 20X magnification. All values are in mean ± SD (n=3 rats/ group). $^{a}p<0.05$, $^{b}p<0.05$, $^{c}p<0.05$, $^{d}p<0.05$, $^{e}p<0.05$, and $^{f}p<0.05$ compared to control, CCI, BaBG-1, BaBG-5, BaBG-10, and 45S5-10 respectively. (One-way ANOVA followed by Tukey's multiple comparison post-hoc test)

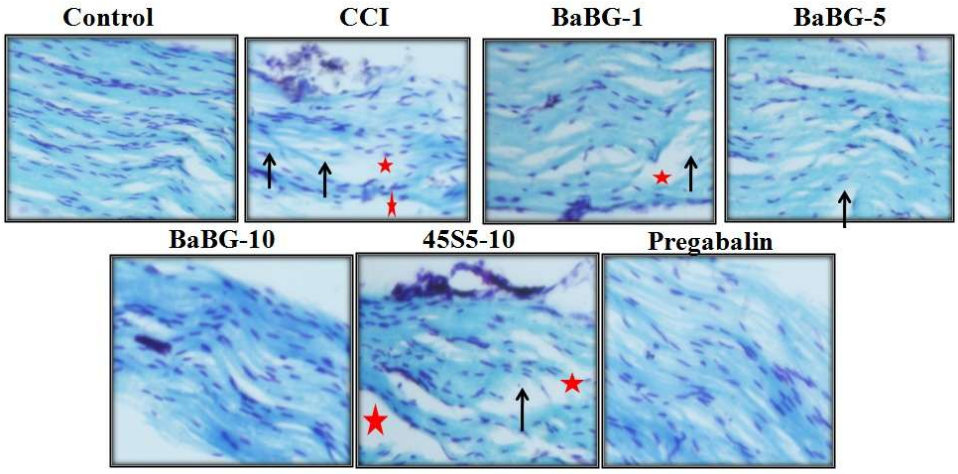

Figure 6.19: Representative image of the histological analyses of SN stained with luxol fast blue at the end of 28th day post-surgery. The arrangement of nerve fibre is disrupted (shown in black arrow) with high degree of myelin vacuolation (red star) in the disease group.

6.2.10. Effect of BaBG on the electrophysiological response upon stimulating the sciatic nerve

Previously, we have observed that following CCI of the SN, there is axonal degeneration causing loss of myelin layer from the SN as reported in **Figures 6.18** and **6.19**. In line with our observation, studies have corroborated these changes in the CCI model of NP that lead to alterations in the electrophysiological response and peripheral nerve functions (Chan, Tsai et al. 2022). Therefore, we have examined the effect of BaBG on the amplitude and latency of the onset of CAP along with its conduction velocity following CCI injury (**Figure 6.20**). One-way ANOVA represented significant alteration in the amplitude, latency of CAP, and MNCV among the groups ([$F(6,34) = 64.69$; $p<0.05$], [$F(6,34) = 396.4$; $p<0.05$],and ([$F(6,34) = 48.01$; $p<0.05$] respectively on D-28 of the experimental protocol. Post-hoc analysis demonstrated that the CCI of the SN caused a significant reduction in the amplitude of CAP and MNCV (2.0 ± 0.71 mV and 19.0 ± 2.91 m/s respectively) compared to the control group i.e., 13.4 ± 2.41 mV and 45.2 ± 4.43 respectively (**Figure 6.20A and C**). Similarly, there was a substantial increase in the latency of onset of CAP (2.92 ± 0.108 ms) in the nerve-injured group than the control rats (1.61 ± 0.078 ms) (**Figure 6.20B**). The reduction in conduction velocity can be ascribed to the loss of the myelin layer resulting from axonal atrophy, which aligns with the findings of investigations conducted on rats (Foudah, Alqarni et al. 2022). Although the MNCV has decreased, the presence of mechanical and cold allodynia indicates a surge in peripheral nerve sensitivity. The hypersensitivity found in this paradigm can be attributable to the heightened expression of VGCC and TRPV1, leading to an increase in intracellular calcium levels as shown in **Figure 6.8**. This rise in calcium levels is essential for maintaining action potential (Helmchen, Borst

et al. 1997, Liu, Xiong et al. 2020). However, treatment with various doses (1, 5, and 10 mg/kg) of BaBG effectively mitigated the CCI-induced changes in the electrophysiological parameters in rats. In addition, the effect of BaBG at the dose of 10 mg/kg (amplitude = 11 ± 1.41 mV, latency = 1.67 ± 0.05 ms, and MNCV = 40.02 ± 3.57 m/s) was more pronounced compared to the moderate and lowest dose of BaBG i.e., 5 and 1 mg/kg. Nevertheless, when given at a dose of 10 mg/kg, the administration of 45S5 was found to be ineffective in the CCI model in alleviating the amplitude and conductive velocity of CAP generated upon stimulating the nerve (amplitude = 1.2 ± 0.44 mV, latency = 2.89 ± 0.073 ms, and MNCV = 19.61 ± 2.71 m/s). Further, the CCB i.e., pregabalin (amplitude = 11.6 ± 1.67 mV, latency = 1.74 ± 0.033 ms, and MNCV = 35.28 ± 3.42 m/s) was found to be comparable to the highest dose of BaBG.

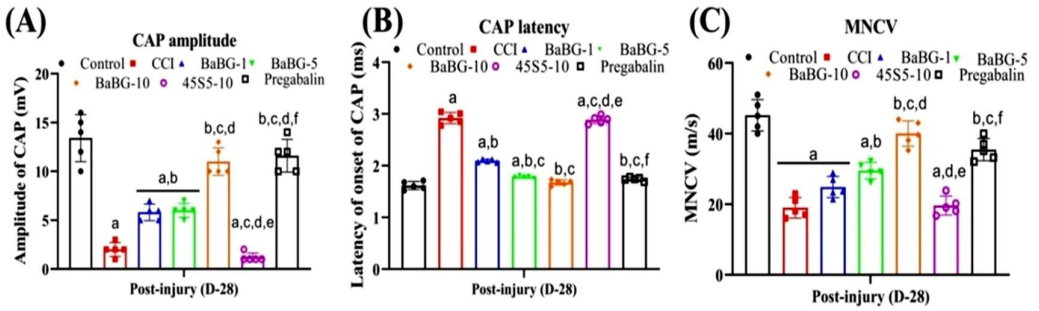

Figure 6.20: Effect of BaBG on (A) amplitude, (B) latency of CAP, and (C) MNCV. All values are in mean ± SD (n=5 rats/ group). [a]p<0.05, [b]p<0.05, [c]p<0.05, [d]p<0.05, [e]p<0.05, and [f]p<0.05 compared to control, CCI, BaBG-1, BaBG-5, BaBG-10, and 45S5-10 respectively. (One-way ANOVA followed by Tukey's multiple comparison post-hoc test)

6.2.11. Effect of BaBG on the muscle functioning in response to the cold-stimulus-evoked allodynia

The alterations in nocifensive reflexes in response to the cold stimuli have been recorded from the gastrocnemius muscle using EMG recordings, as depicted in **Figure 6.21**. The withdrawal response is noticed when a noxious stimulus, such as a cold

sensation from acetone dropped on an injured paw, is present. This reflex is due to the function of the gastrocnemius muscle to lower limb flexion. We observed that the control rats had a longer delay in the flexor EMG response compared to the CCI group, and the magnitude of the EMG was less when acetone was dropped on the rats' paws. However, the flexor EMG response of the CCI group exhibited a lower threshold and prolonged afterdischarges, as depicted in **Figure 6.21**; CCI. This observation is consistent with previous findings in the CCI model of NP (Bennett and Xie 1988); suggesting an exaggerated sensitivity to cold stimuli that are not normally painful and the occurrence of cold allodynia. Nevertheless, following the administration of BaBG, there was a decrease in the magnitude of EMG and after discharges in response to acetone stimulation, suggesting alleviation of CCI-induced sensory hypersensitivity. The EMG recording from the 45S5-treated group exhibited a reduction in the magnitude of discharges post-acetone stimulation without much difference in after discharges observed during flexion of the gastrocnemius muscle. Therefore, we can conclude that BaBG alleviated CCI-induced cold allodynia that corroborates the pain behavioral assessment tests as shown in **Figure 6.6**.

6.2.12. Effect of BaBG on the gastrocnemius muscle post-CCI injury

The gastrocnemius muscle, innervated by branches of the sciatic nerve, is the major muscle responsible for knee flexion and assisting in overall body movement. Denervated muscles have a loss of signal transmission from the nervous system, resulting in an inability to sustain contraction. As a result, damage to the SN is known to result in immobility or decreased function of the injured limb clinically and preclinically leading to muscle atrophy (Choe, Kim et al. 2011, Bhindi, Angliss et al. 2022). Further, there are reports of reduced muscular protein synthesis and an increase in protein breakdown, causing myatrophy and reduced thegastrocnemius muscle weight (Wang, Chen et al. 2021) as observed in our study in **Figure 6.22**. Following a CCI

injury, there was a notable decrease in the weight of the gastrocnemius muscle of the ipsilateral side of CCI rats (i.e., 0.488±0.1178g) compared to the control rats i.e., 1.49 ± 0.109, indicating muscle atrophy (**Figure 6.22**). One-way ANOVA demonstrated significant changes in the muscle weight among groups ([$F(6, 41) = 61.77$; $p < 0.05$] (**Figure 6.22**). The Tukey's post hoc test revealed that following the injury to the peripheral nerve, the weight of gastrocnemius muscle had reduced significantly in the CCI group compared to naïve rats which was reversed following BaBG treatment in a dose-dependent manner ($p < 0.05$). Pregabalin (30 mg/kg) treatment also reversed the CCI-induced muscle weight decrease but was significantly less potent compared to the highest dose of BaBG. Similarly, 45S5 (10 mg/kg) did not show any changes in the gastrocnemius muscle weight compared to the CCI rats.

Similarly, thehistological analyses of the H & E stained gastrocnemius muscle post-CCI revealed muscle atrophy. The control rats exhibited homogeneous morphology with densely packed acidophilic polygonal-shaped skeletal muscle fibres and the peripheral nuclei are ovalin shape as shown in **Figure 6.22**.While in the CCI group, there was fragmentation of the sarcoplasm (shown in black arrow) with the mononuclear cell infiltration (**Figure 6.22)**. We also observed a widening of the endomysium in the injured rats (shown in black stars) and some of them exhibited vacuolations (red arrow) However, treatment with BaBG significantly increased the gastrocnemius muscle fiber cross-section area. The fiber cross-section area of the highest dose of BaBG (10mg/kg) treated ratswas increased to 70.16 ± 4.16% from 38.83 ± 4.30 % as observed in CCI rats. In the pregabalin (30 mg/kg) and 45S5 (10 mg/kg) treated rats, the gastrocnemius muscle fiber cross-section area was found to be 54.33 ± 3.82 and 47.66 ± 3.92 % respectively which was significantly lesser than BaBG (10 mg/kg). In light of these findings, it can be inferred that motor impairments are closely linked to the CCI model of NP and BaBG treatment reversed all core symptoms of NP along with the observed motor impairment.

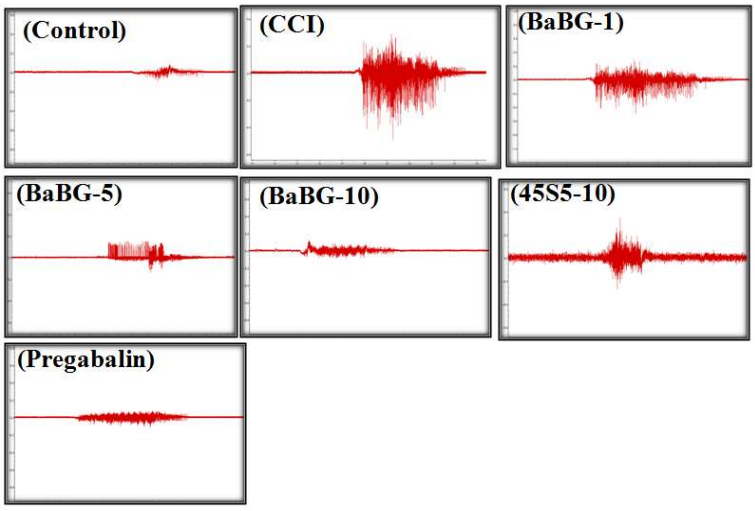

Figure 6.21: Representative images of the EMG recording in response to the cold-stimulus-evoked allodynia in control, CCI, BaBG-1, BaBG-5, BaBG-10, 45S5-10, and pregabalin treated rats.

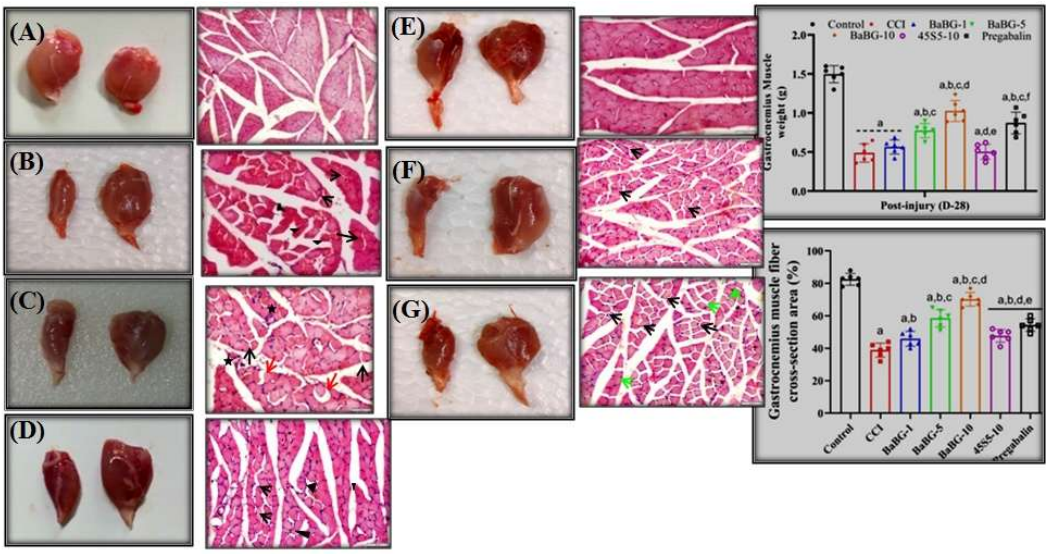

Figure 6.22: Representative images of the gastrocnemius muscle of the contralateral and ipsilateral side of the leg along with the histological analyses of gastrocnemius muscle stained with hematoxylin and eosin at the end of experimental protocol. Effect of BaBG on gastrocnemius muscle weight and cross-section area of muscle fiber. All values are in mean ± SD (n=5 rats/ group). $^{a}p<0.05$, $^{b}p<0.05$, $^{c}p<0.05$, $^{d}p<0.05$, $^{e}p<0.05$, and $^{f}p<0.05$ compared to control, CCI, BaBG-1, BaBG-5, BaBG-10, and 45S5-10 respectively. (One-way ANOVA followed by Tukey's multiple comparison post-hoc test)

6.3. Conclusion

The current findings establish that BaBG exhibits a significant effect in mitigating the CCI-induced sensory hypersensitivity and the characteristic motor impairments observed in NP. Calcium ions play a crucial role in neuronal signaling and excitability, and dysregulation of calcium homeostasis has been implicated in NP. In the *ex vivo* electrophysiological setup, BaBG prolonged the repolarization phase of action potential in the SN. Consequently, BaBG decreased the propagation of action potential and under NP circumstances; there is heightened sensitivity of nociceptors observed. Further, BaBG reversed all NP symptoms in a dose-dependent manner in the CCI model in rats. It also hindered the activation of S100b and decreased inflammation post-CCI of peripheral nerve. Treatment with BaBG caused axonal repair and remodeling of the dendrites. Similar to pregabalin, BaBG attenuated the elevated intracellular calcium levels in the SN and SC post-injury in rats. Notably, these effects exhibit a dose-dependent relationship, with 10 mg/kg proving to be the most effective dose compared to 1 and 5 mg/kg. In conclusion, these findings provide compelling evidence supporting the calcium-regulating potential of BaBG, thus potentially impeding calcium-associated NP pathogenesis.

Summary

- ❖ BaBG has the calcium regulating potential.
- ❖ BaBG reduced the intracellular calcium level in the sciatic nerve and spinal cord post-CCI injury in a dose-dependent manner.
- ❖ It ameliorated the CCI-induced sensory hypersensitivity (hyperalgesia and allodynia).
- ❖ The motor deficits caused due to the CCI were alleviated by BaBG in a dose-dependent manner.

- ❖ BaBG also lowered the S100b expression and pro-inflammatory marker level in the sciatic nerve and spinal cord post-peripheral nerve injury.
- ❖ Treatment with BaBG improved the compound action potential conduction velocity and amplitude which was comparable to the pregabalin treated group.
- ❖ BaBG treatment caused axonal repair and remyelination in dose-dependent manner.
- ❖ BaBG caused dendritic arborization, a mechanism contributing to neuronal connectivity and communications that helps in functional recovery.

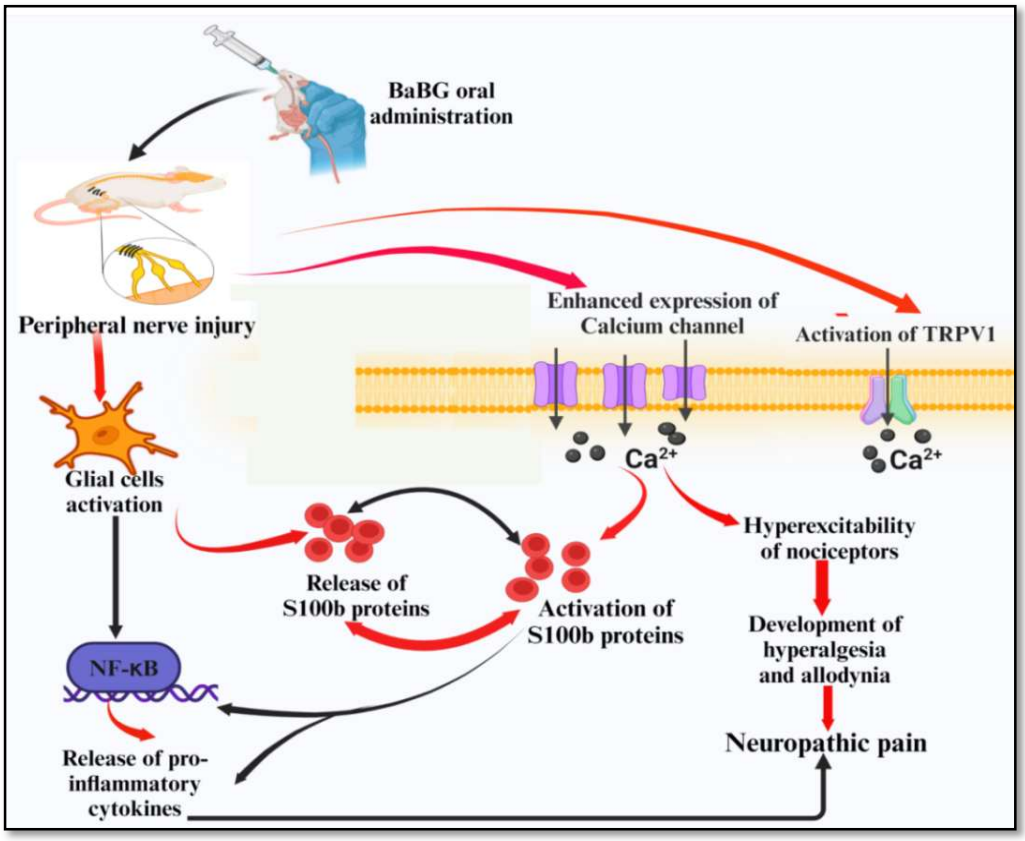

Figure 6.23 Showcases the specific objective's outcome in exploring the molecular mechanism behind the effect of BaBG in attenuating neuropathic pain (NP) in a CCI-induced NP rat model. It suggests that the development and progression of NP is associated with the enhanced calcium channel and TRPV1 expression that caused increase in the intracellular calcium and calcium-binding protein i.e., S100b level. These events led to glial cell activation that releases cytokine storm, thus exaggerating

NP sensation. BaBG exhibited novel calcium regulating mechanism as it prolonged the repolarization phase of action potential. The Treatment with BaBG significantly reversed the NP phenotypes induced by CCI. Besides, CCI of peripheral nerve caused glial cell hyperactivation that was attenuated by BaBG. BaBG also lowered the S100B-induced increase in pro-inflammatory markers, specifically TNF-α and IL-6, in both the SC and SN post-injury.